nature cardiovascular research

Article

https://doi.org/10.1038/s44161-025-00724-z

B cells promote atrial fibrillation via autoantibodies

Received: 9 February 2024

Accepted: 28 August 2025

Published online: 8 October 2025

Check for updates

Masahiro Yamazoe[1,2], Kenneth K. Y. Ting[1,2], I-Hsiu Lee[1,2], Aneesh Bapat[3], Andrew Lewis[4,5], Ling Xiao[3,6], Fadi E. Pulous[1,2], Kyle Mentkowski[1,2], Alexandre Paccalet[1,2], Noor Momin[1,2], Hana Seung[1,2], Theresa Dolejsi[1,2], Nina Kumowski[1,2], Maximilian J. Schloss[1,2], Yoshiko Iwamoto[1,2], Gustavo Ramos[7], Kenneth Chan[4], Charalambos Antoniades[4], Barbara Casadei[4,5], Filip K. Swirski[8,9], Patrick T. Ellinor[3,6], Kamila Naxerova[1,10], Steffen Pabel[1,2,11,13] ✉, Maarten Hulsmans[1,2,13] ✉ & Matthias Nahrendorf[1,2,3,7,12,13] ✉

Atrial fibrillation, the most frequent cardiac arrhythmia, causes heart failure and stroke. Here we describe that combining the typical risk factors of atrial fibrillation (hypertension, obesity and mitral valve regurgitation (HOMER)) activates adaptive immunity in wild-type mice, ultimately causing electrical remodeling of cardiomyocytes. In HOMER mice, dendritic cells expanded in the left atria and heart-draining lymph nodes, where we detected cardiomyocyte-derived proteins. Systemically expanding B cells, while exposed to interferon-α, produced autoantibodies that disrupted calcium handling in cardiomyocytes. Depleting B cells by using μMT HOMER mice or plasma cells by using *Mb1*$^{cre/+}$ *Prdm1*$^{fl/fl}$ HOMER mice reduced atrial fibrillation while mitigating the prolonged action potential duration we observed in the left atria of HOMER mice. CD20 antibody B cell depletion, a clinical tool in treating lymphoma and autoimmune disease, reduced atrial fibrillation fivefold in HOMER mice. Targeting humoral immunity may provide therapeutic avenues for patients with autoantibody-induced atrial fibrillation.

Atrial fibrillation (AF) is the most frequent sustained arrhythmia and leads to heart failure and thromboembolic stroke, thus causing considerable mortality and morbidity[1]. The socioeconomic consequences of AF are significant and insufficiently managed[2]. Among standard treatment options, cardioversion, catheter ablation or antiarrhythmic drug therapy can restore sinus rhythm, but AF often reoccurs[3]. Anticoagulation, which prevents thromboembolic stroke, carries bleeding risks. Hence, a better understanding of pathways that elicit AF is urgently needed to develop effective and safe therapeutics.

Leukocytes, a recently identified addition to the atrial resident cell map, can influence the structural properties of the heart's extracellular space[4,5]. For instance, recruited SPP1^{+} macrophages promote the atrial arrhythmogenic substrate through pleiotropic effects on inflammation and fibrosis[5], thereby increasing conduction heterogeneity such that electrical re-entry circuits form. Altered myocardial calcium handling is another pathophysiological hallmark of incident AF, but whether and how leukocytes contribute to it is unclear. Dendritic cells (DCs) and lymphocytes, adaptive immune cell classes that interact during B cell maturation and antibody production, reside in the healthy and diseased hearts of both mice[6] and humans[7,8]. DCs such as conventional DCs (cDCs) are critical responders to infection and injury and coordinate adaptive immunity by presenting antigens to lymphocytes, which then produce antibodies[9]. Autoantibodies have been observed in individuals with cardiomyopathy[10] and AF[11]. Specifically, autoantibodies against

A full list of affiliations appears at the end of the paper. ✉e-mail: steffen.pabel@gmail.com; mhulsmans@mgh.harvard.edu; mnahrendorf@mgh.harvard.edu

https://doi.org/10.1038/s44161-025-00724-z

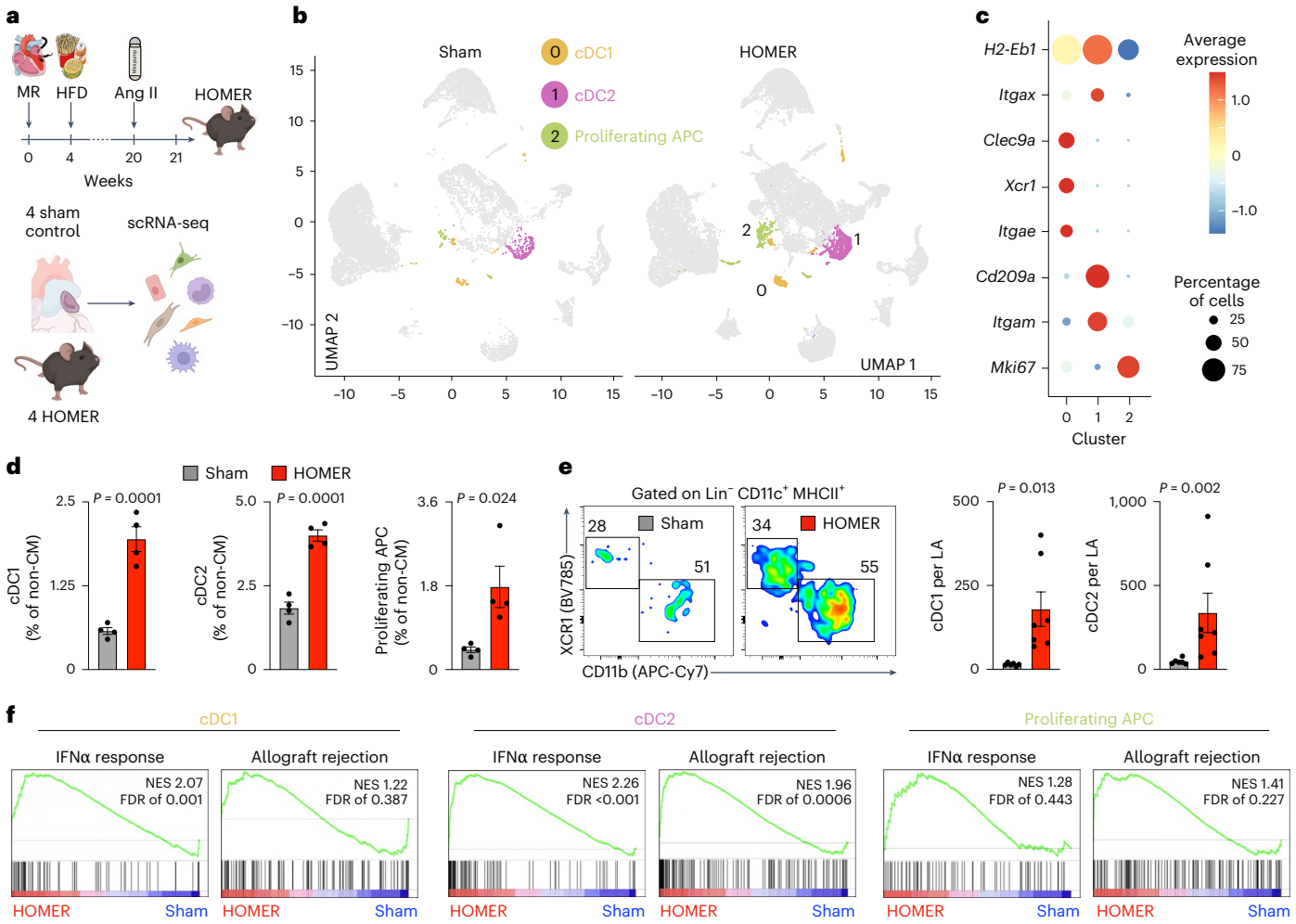

Fig. 1 | DC expansion in left atria from HOMER mice. a, Experimental outline: scRNA-seq of four sham and four HOMER atria. Ang II, angiotensin II; HFD, high-fat diet; MR, mitral valve regurgitation. **b**, Uniform manifold approximation and projection (UMAP) plot highlighting DCs and proliferating APCs. **c**, Dot plot annotating cDC1, cDC2 and proliferating APCs by signature gene expression. The color denotes the *z*-score of average gene expression and circle size indicates percentage of cells expressing the gene. **d**, The frequency of cDC1 (cluster 0), cDC2 (cluster 1) and proliferating APCs (cluster 2) in the atria of four sham and four HOMER mice identified by scRNA-seq. CM, cardiomyocyte. Each dot indicates a biological replicate. **e**, Flow cytometric quantification of left atrial (LA) cDC1 (left) and cDC2 (right) in sham and HOMER mice. $n = 6$ and $n = 7$ per group. **f**, Enriched gene sets for cDC1, cDC2 and proliferating APCs. NES, normalized enrichment score. *P* values determined by two-tailed Student's *t*-test (**d**) or two-tailed Mann–Whitney test (**e**). Data are the mean ± s.e.m. with individual values for data distribution.

the M_2 muscarinic acetylcholine receptor and the β_1 adrenergic receptor have been associated with AF[12,13] and may cause atrial arrhythmia in animals[14].

This work identifies the contributions of DCs and lymphocytes to atrial health, myocardial calcium handling and arrhythmia. We demonstrate that common AF risk factors give rise to autoantibodies against membrane proteins expressed by atrial cardiomyocytes. These antibodies trigger proarrhythmic electrophysiological phenotypes that can be suppressed by B cell depletion and inhibition of plasma cell maturation.

Results

Left atrial DCs expand in AF

To examine adaptive immune cell contributions to AF, we relied on a recently established, well-validated inducible AF mouse model that combines three common clinical risk factors: hypertension, obesity and mitral valve regurgitation (HOMER)[5] (Fig. 1a). In this model, mitral valve regurgitation is induced by placing a suture through the posterior mitral valve leaflet[5]. Previously acquired single-cell RNA sequencing (scRNA-seq) data from sham and HOMER mice showed high left atrial frequencies of mononuclear phagocytes and DCs[5]. Using typical marker genes, we identified three DC subclusters including type 1 and type 2 cDCs (cDC1 and cDC2, respectively) and proliferating antigen-presenting cells (APCs) (Fig. 1b,c). All three clusters were significantly more frequent in HOMER atria when compared with normotensive, sham-operated controls that consumed a chow diet (Fig. 1d). By flow cytometry, we confirmed the substantially increased left atrial cDC1 and cDC2 in HOMER mice (Fig. 1e). Two of the three DC clusters, specifically cDC1 and cDC2, significantly enriched for the gene set 'interferon-α (IFNα) response' in HOMER atria (Fig. 1f). IFNα enhances DC maturation and migration[15] and has a key role in autoimmune diseases such as systemic lupus erythematosus, specifically by promoting differentiation to autoreactive B cells and autoreactive plasma cells which then produce autoantibodies[16]. Notably, the HOMER cDC2 cluster also enriched for the gene set 'allograft rejection' (Fig. 1f). Consistent with HOMER mice, we identified two distinct DC subclusters, DC(a) and DC(b), in five control participants and seven patients with persistent AF undergoing heart surgery[5] (Fig. 2a–d). In patients with AF, both DC clusters were enriched for the IFNα response gene set compared with controls (Fig. 2e), recapitulating our mouse findings.

https://doi.org/10.1038/s44161-025-00724-z

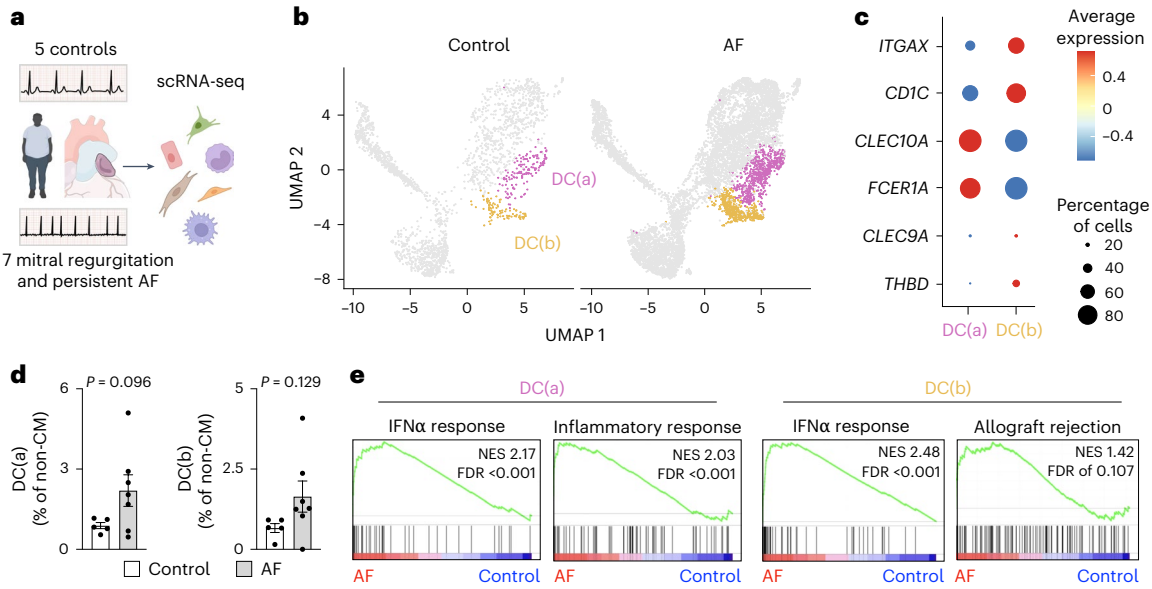

Fig. 2 | DC expansion in left atria from patients with AF. a, Experimental outline illustrating scRNA-seq analysis of noncardiomyocytes isolated from left atrial appendages of five control individuals and seven individuals with mitral valve regurgitation and persistent AF. **b**, UMAP plot highlighting left atrial DCs in the mononuclear phagocytes and DC subcluster from five controls and seven individuals with AF. **c**, Dot plot annotating DCs by signature gene expression. The color denotes the *z*-score of average gene expression and circle size indicates percentage of cells expressing the gene. **d**, DC subset frequency in left atria from five controls and seven individuals with AF by scRNA-seq. **e**, Gene sets enriched in DC from the left atria of individuals with AF. *P* values determined by two-tailed Student's *t*-test. Data are the mean ± s.e.m. with individual values for data distribution.

Because we observed DC expansion, we next evaluated the lymphocytes they frequently interact with. We compared atrial B cell gene expression between sham and HOMER mice and identified 171 differentially expressed genes (DEGs) with a false discovery rate (FDR) of less than 0.05 (Extended Data Fig. 1a). We used gene set enrichment analysis (GSEA) to compare all atrial B cells in HOMER and sham controls (Extended Data Fig. 1b,c). In atrial B cells of HOMER mice, we observed an enrichment in gene sets that were generally related to B cell activation and inflammation but more specifically to antigen presentation and immunoglobulin-mediated immune responses (Extended Data Fig. 1b,c). In addition to allograft rejection, we also detected significant enrichment of the gene set 'oxidative phosphorylation' (Extended Data Fig. 1c), which B cells switch to when they proliferate and differentiate to antibody-producing cells[17]. Reclustering atrial B cells yielded four B cell subsets, including one B1 and three B2 B cell clusters (Extended Data Fig. 1d–f). B2 B cells included separate clusters of transitional and mature B cells, reflecting stages of B cell maturation. GSEA of these B cell subsets revealed that in HOMER atria, B2 B cells (that is, B cell clusters 1, 2 and 3) upregulated pathways associated with antigen presentation and IFNα response (Extended Data Fig. 1g).

Finally, we studied the T cell response in our scRNA-seq data from HOMER atria. We found 104 DEGs (FDR < 0.05) (Extended Data Fig. 2a) when comparing all atrial T cells between control and HOMER mice. Aligning with adaptive immune response pathways we describe above in DCs and B cells, GSEA highlighted upregulated inflammatory pathways including humoral immune and IFNα response in T cells residing in HOMER atria (Extended Data Fig. 2b,c). Of the five T cell clusters identified, cell frequencies were comparable between control and HOMER atria with the exception of ILC2, which were lower in HOMER mice (Extended Data Fig. 2d–f). GSEA in individual T cell clusters showed activation of inflammatory signaling in HOMER atria (Extended Data Fig. 2g). Together, these data indicate that adaptive immune cells are activated in the atria of HOMER mice; however, this may reflect systemic activation. Furthermore, the total number of adaptive immune cells identified in HOMER atria, which may be influenced by cell retrieval and survival, was relatively low. Of note, cardiac tissue is unlikely the primary site of adaptive immune activity, which is why we next studied heart draining lymph nodes.

Heart proteins transfer to draining lymph nodes in HOMER mice

Once activated, DCs migrate to draining lymph nodes to orchestrate adaptive immune responses[18]. HOMER mice indeed developed enlarged mediastinal lymph nodes (Fig. 3a,b). To examine mediastinal lymphadenopathy in individuals with AF, we quantified lymph node size in sinus rhythm versus individuals with AF who underwent cardiac computed tomography (Fig. 3c and Supplementary Table 1). Consistent with HOMER mice, individuals with AF had larger mediastinal lymph nodes than individuals with sinus rhythm (Fig. 3d). In mediastinal lymph nodes, among MHCII^{high} DCs, which are typically considered migratory DCs[19], cDC2 were more numerous in HOMER mice compared with controls, whereas cDC1 were not changed (Fig. 3e). Together, these findings support a role for cDC2 atrial antigen presentation in HOMER mice.

Motivated by the enrichment of the gene set IFNα response gene set in atrial DCs of HOMER mice and individuals with AF (Fig. 1f and Fig. 2e), we next examined the *Ifna* gene expression in mediastinal lymph nodes. *Ifna* expression increased in mediastinal lymph nodes of HOMER mice (Fig. 3f), which also had more serum IFNα protein (Fig. 3g). Since plasmacytoid DCs (pDCs) are the main source of IFNα[20], we examined whether pDCs expanded in mediastinal lymph nodes and left atria of HOMER mice. Indeed, pDC numbers rose both in mediastinal lymph nodes and left atria of HOMER mice (Fig. 3h,i).

To explore whether cardiomyocyte membrane components drain to lymph nodes, we assayed eGFP signal in DCs isolated from mediastinal lymph nodes of *Myh6*$^{cre/+}$ *mTmG*$^{fl/+}$ HOMER mice, comparing them to sham-operated *Myh6*$^{cre/+}$ *mTmG*$^{fl/+}$ mice (Fig. 3j). In HOMER mice, activated enhanced green fluorescent protein-expressing (eGFP^{+}) DCs expanded in mediastinal lymph nodes, indicating transfer of cardiomyocyte-derived protein to antigen presentation sites (Fig. 3k,l). Viewed together, our data support myocyte-derived protein transport to draining lymph nodes with enhanced IFNα signaling in HOMER mice, suggesting adaptive immune activation.

https://doi.org/10.1038/s44161-025-00724-z

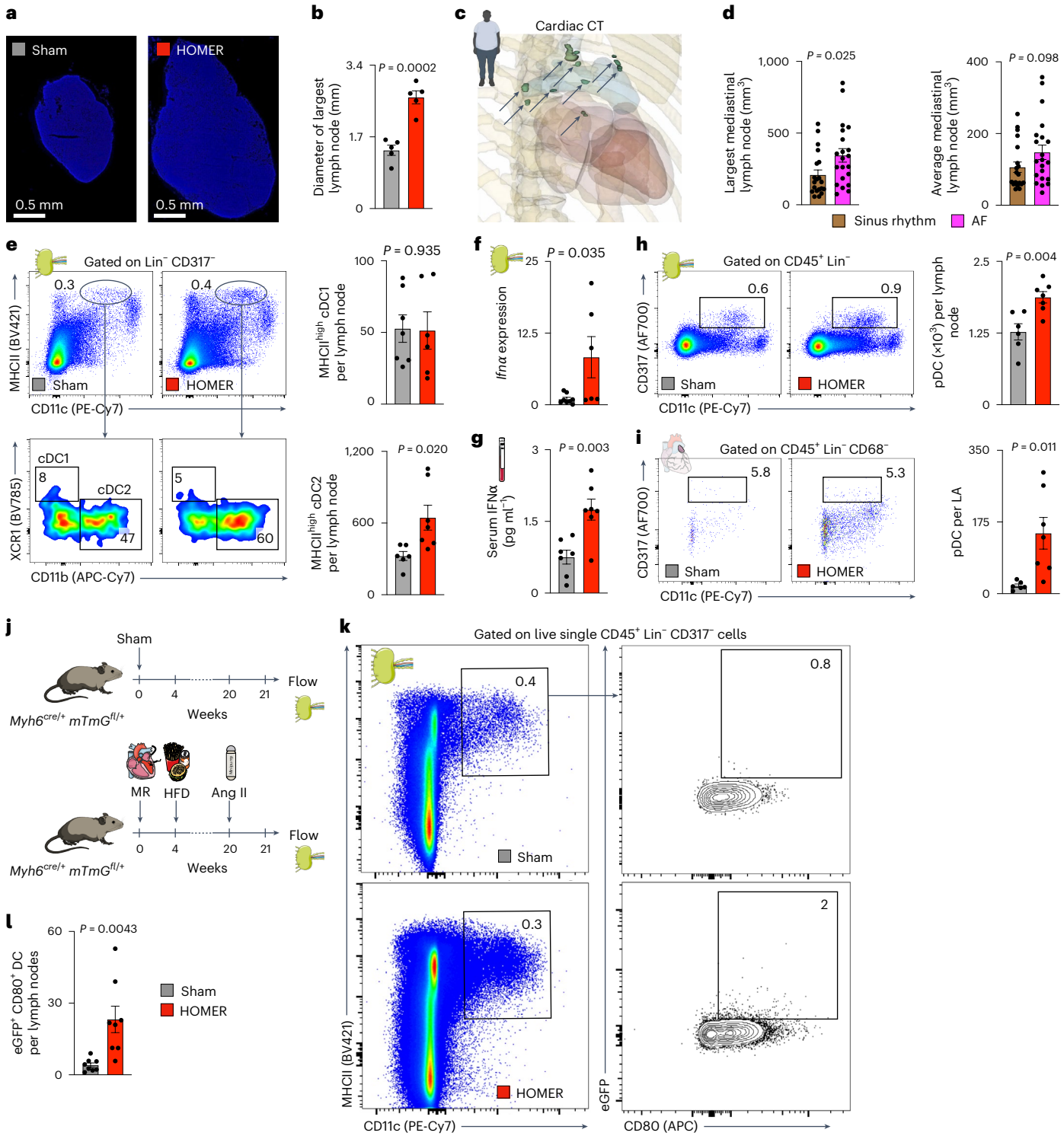

Fig. 3 | DCs in heart draining lymph nodes. a, Representative mediastinal lymph node from sham and HOMER mice stained with DAPI (4′,6-diamidino-2-phenylindole). **b**, Quantification of the largest mediastinal lymph node diameter from sham and HOMER mice. $n = 5$ per group. **c**, Representative three-dimensional mediastinal lymph node segmentation of a patient undergoing cardiac computed tomography (CT). Black arrow denotes mediastinal lymph nodes. **d**, The quantified largest (left) and average (right) lymph node size in sinus rhythm ($n = 20$) and individuals with AF ($n = 21$). **e**, Flow cytometric quantification of MHCII^{high} cDC1 and cDC2 in mediastinal lymph nodes from sham and HOMER mice. $n = 6$ and $n = 7$. **f**, Expression of *Ifn* in mediastinal lymph nodes from sham and HOMER mice quantified by qPCR. $n = 6$ and $n = 8$ per group. **g**, Serum IFNα protein levels in sham and HOMER mice. $n = 7$ per group. **h**, Flow cytometric quantification of pDCs in mediastinal lymph nodes from sham and HOMER mice. $n = 6$ and $n = 7$ per group. **i**, Flow cytometric quantification of pDCs in left atria from sham and HOMER mice. $n = 6$ and $n = 7$ per group. **j**, Experimental outline using *Myh6*$^{cre/+}$ *mTmG*$^{fl/+}$ sham and HOMER mice. **k**,**l**, Representative flow cytometry plots (**k**) and quantification (**l**) of activated CD80$^+$ eGFP$^+$ DCs in mediastinal lymph nodes from *Myh6*$^{cre/+}$ *mTmG*$^{fl/+}$ sham and HOMER mice. $n = 8$ mice per group. *P* values determined by two-tailed Student's *t*-test (**a**,**e**–**i**,**l**) or two-tailed Mann–Whitney test (**d**). Data are the mean ± s.e.m. with individual values for data distribution.

https://doi.org/10.1038/s44161-025-00724-z

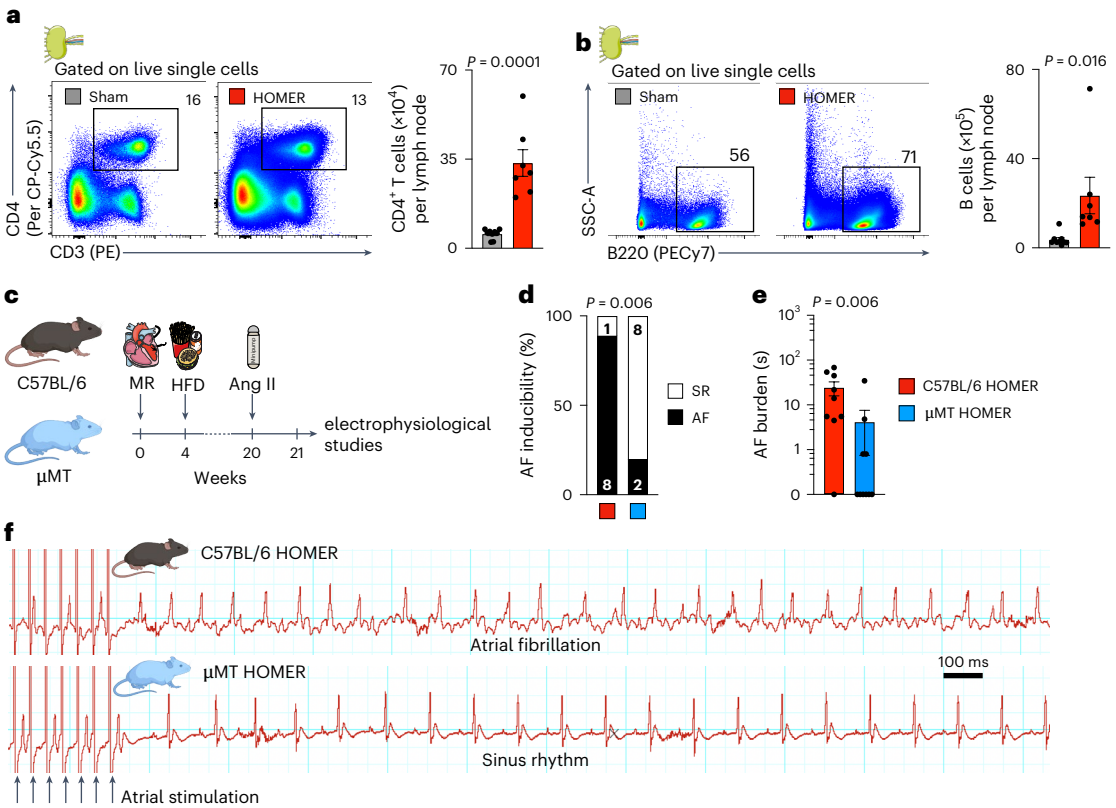

Fig. 4 | Expanding B cells promote AF. a, Flow cytometric quantification of $CD4^+$ T cells in mediastinal lymph nodes from sham and HOMER mice. $n = 9$ and $n = 7$. **b**, Flow cytometric quantification of B cells in mediastinal lymph nodes from sham and HOMER mice. $n = 9$ and $n = 7$ per group. **c**, Experimental outline: C57BL/6 and B cell knockout (µMT) HOMER mice were analyzed in an invasive electrophysiological study. **d**, AF inducibility in C57BL/6 and µMT HOMER mice. $n = 9$ and $n = 10$ per group. SR, sinus rhythm. **e**, AF burden in C57BL/6 and µMT HOMER mice. $n = 9$ and $n = 10$ per group. **f**, Representative ECG after rapid atrial stimulation in C57BL/6 and µMT HOMER mice. *P* values determined by two-tailed Student's *t*-test (**a**,**b**), two-sided Fisher's exact test (**d**) or two-tailed Mann–Whitney test (**e**). Data are the mean ± s.e.m. with individual values for data distribution.

Expanding B cells promote AF

Activated DCs carrying antigen license $CD4^+$ T cells, which then help B cells to proliferate[18]. Accordingly, $CD4^+$ T cells and B cells both expanded in mediastinal lymph nodes of HOMER mice (Fig. 4a,b). The expansion of B cells was present across different subsets in mediastinal lymph nodes and to a lesser extent in the spleen (Extended Data Fig. 3a–m). Specifically, plasma cells, plasmablasts and follicular B cells expanded in the heart draining lymph nodes of HOMER mice (Extended Data Fig. 3d–g). To investigate whether the observed B cell expansion causally contributes to AF, we subjected C57BL/6 wild-type and µMT mice, which lack B cells, to the HOMER risk factors (Fig. 4c). Circulating leukocytes were lower in µMT HOMER mice due to the lack of B cells, as expected, while blood myeloid cells were similar in C57BL/6 HOMER and µMT HOMER mice (Extended Data Fig. 4a). T cells were more numerous in µMT mice, but this observation was independent of the HOMER protocol (Extended Data Fig. 4a,b). Invasive EP studies revealed fivefold lower AF inducibility and AF burden in µMT HOMER mice compared with C57BL/6 HOMER mice (Fig. 4d–f). Body weight and blood pressure did not differ between C57BL/6 HOMER and µMT HOMER mice (Extended Data Fig. 4c,d), excluding the possibility that the drastic AF reduction in µMT HOMER mice was confounded by an effect of B cell depletion on AF risk factors.

Plasma cells and IgM increase in HOMER mice

B cells give rise to plasma cells which expanded in the heart draining lymph nodes of HOMER mice (Extended Data Fig. 3d). In a time-course analysis spanning the exposure to all HOMER components, we observed a plasma cell expansion before angiotensin II infusion at 20 weeks, which remained increased thereafter (Extended Data Fig. 5a). Within the germinal center of lymph nodes, B cells undergo somatic hypermutation and interact with follicular helper T cells to differentiate into long-lived plasma cells[21]. In mediastinal lymph nodes of HOMER mice, germinal center B cell numbers did not change significantly (Extended Data Fig. 5b), while follicular helper T cells expanded compared with controls (Extended Data Fig. 5c). In the bone marrow, plasma cells of HOMER mice did not increase, suggesting that the HOMER protocol did not significantly affect long-lived plasma cells at the studied time point (Extended Data Fig. 5d).

Consistent with expanded plasma cells in mediastinal lymph nodes (Extended Data Fig. 5a), serum IgM increased in HOMER mice, reaching significantly higher levels than in controls at 1, 20 and 21 weeks after the model was initiated (Fig. 5a and Extended Data Fig. 5e). To test the hypothesis that the observed autoantibody response relies on presentation of heart antigen, we applied the HOMER protocol to *MHCII*$^{-/-}$ (also known as *H2*$^{-/-}$) mice[22] (Extended Data Fig. 5f). HOMER mice lacking MHCII had lower blood IgM levels compared with C57BL/6 HOMER mice (Extended Data Fig. 5g). We then specifically tested the role of DCs by depleting them using diphtheria toxin in *Cd11c*^{DTR} mice[23] (Extended Data Fig. 5h). Because mice survive DC depletion only for a short time period[23], we evaluated IgM levels 1 week after diphtheria toxin injection and mitral valve regurgitation surgery, the first component of the HOMER protocol. Interestingly, *Cd11c*^{DTR} mice with mitral valve regurgitation had decreased IgM levels compared with C57BL/6 mice with mitral valve regurgitation (Extended Data Fig. 5i). IgG serum levels were not significantly higher

https://doi.org/10.1038/s44161-025-00724-z

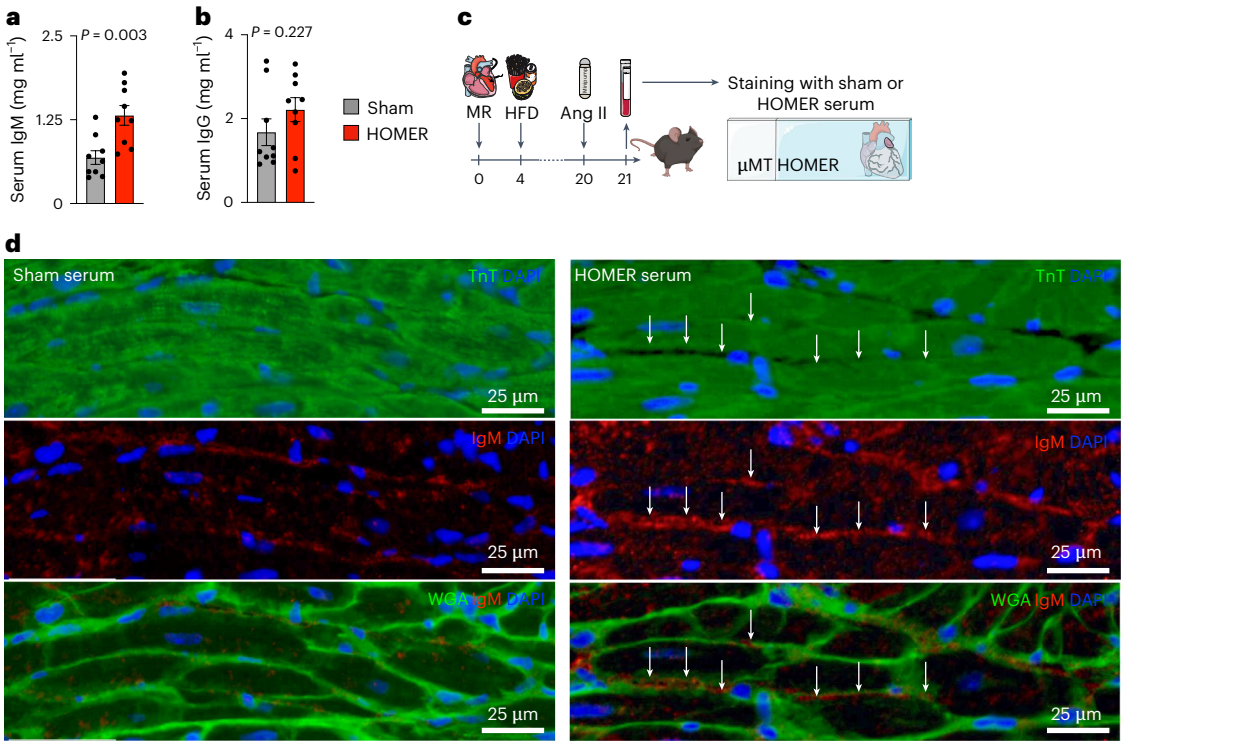

Fig. 5 | Plasma cells expand in HOMER mice and deposit IgM in atria. a,**b**, Serum levels of IgM (**a**) and IgG (**b**) in sham and HOMER mice quantified by ELISA. $n = 9$ per group **c**, Experimental outline: sham or HOMER mice serum was applied to µMT HOMER atrial sections and detected by anti-IgM antibody staining. **d**, A representative staining of IgM in µMT HOMER left atria with C57BL/6 sham and HOMER serum. Costaining with wheat-germ agglutinin (WGA) and troponin T (TnT) for cell membranes and cardiomyocytes, respectively. Arrows indicate IgM deposits on cell membranes. *P* values determined by two-tailed Student's *t*-test. Data are the mean ± s.e.m. with individual values for data distribution.

in HOMER mice compared with controls (Fig. 5b), but rose 4 weeks after the HOMER protocol was completed (Extended Data Fig. 5j,k).

To test whether the antibodies produced in HOMER mice bind to an antigen expressed in atrial tissue, we applied control or HOMER sera to atrial sections obtained from µMT HOMER mice, followed by staining for IgM (Fig. 5c). We chose to assay antibody binding in µMT HOMER tissue because these mice lack IgM; thus, all detected antibody stems from the assayed serum. Compared with serum isolated from controls, HOMER serum led to higher IgM deposition in left atria from µMT HOMER mice (Fig. 5d and Extended Data Fig. 6a). Costaining with troponin T or wheat germ agglutinin showed that IgM in HOMER serum dominantly bound to cardiomyocyte surfaces and not to skeletal muscle (Fig. 5d and Extended Data Fig. 6b). Because HOMER serum contains higher IgM titers than controls, we further assayed IgM cardiomyocyte binding using diluted HOMER serum with IgM concentrations matching those observed in controls. We again detected membrane-associated fluorescence when using HOMER but not control serum (Extended Data Fig. 6c), making unspecific antibody binding less likely. We did not observe IgG binding on cardiomyocyte membranes treated with serum collected immediately after completion of the HOMER protocol (Extended Data Fig. 6d). These data indicate that HOMER sera contain anti-cardiomyocyte IgM.

IgM from HOMER mice disrupts calcium handling in cardiomyocytes

Atrial fibrosis is a frequent arrhythmogenic substrate for AF[24]. Therefore, to assay the atria of C57BL/6 HOMER and µMT HOMER mice, we used Masson's trichrome staining, which revealed no difference in fibrosis-rich areas between these cohorts (Extended Data Fig. 7a,b). Next, we compared electrical properties of cardiomyocytes by assaying their action potential duration using optical mapping of atria in the isolated, retrogradely perfused heart. In left atria of C57BL/6 HOMER mice, we detected longer action potential durations compared with controls. Conversely, µMT HOMER mice exhibited significantly shorter action potentials than C57BL/6 HOMER mice, similar to those of control mice (Fig. 6a,b). We thus hypothesized that IgM in HOMER mice induces electrical remodeling of cardiomyocytes and particularly affects calcium handling, which has a central role in AF induction and maintenance[25]. To test this hypothesis, we incubated neonatal mouse ventricular cardiomyocytes with IgM purified from control or HOMER mice, followed by staining with a fluo-4 calcium indicator. The calcium signal was then recorded by fluorescence microscopy (Fig. 6c). Calcium transients from cardiomyocytes cultured with either control- or HOMER-derived IgM for 24 h differed notably (Fig. 6d). Cardiomyocytes exposed to HOMER-derived IgM for both 1 or 24 h exhibited higher amplitudes and more frequent spontaneous calcium release events compared with cardiomyocytes exposed to IgM isolated from control mice (Fig. 6e,f). Moreover, we observed a longer time-to-peak duration in cardiomyocytes exposed to HOMER-derived IgM for 24 h than those exposed to control IgM with no significant difference in the rate of intracellular calcium decay (Fig. 6g,h). These data suggest that HOMER mice produce IgM that promote atrial arrhythmia by disturbing calcium handling. Indeed, isolated adult atrial cardiomyocytes from HOMER mice show disturbed calcium transients and increased proarrhythmic calcium release events compared with sham controls (Extended Data Fig. 8).

To ascertain to what degree immunoglobulins are responsible for inducible AF differences between C57BL/6 HOMER and µMT HOMER mice, we transferred purified control or HOMER IgM to µMT HOMER mice (Extended Data Fig. 9a). µMT HOMER mice injected with HOMER IgM had a higher AF burden compared with µMT HOMER mice injected with control IgM (Extended Data Fig. 9b,c). Given these antibody-mediated effects, we next studied B cell differentiation to plasma cells by applying the HOMER protocol to $Mb1^{cre/+}$ $Prdm1^{fl/fl}$ mice.

https://doi.org/10.1038/s44161-025-00724-z

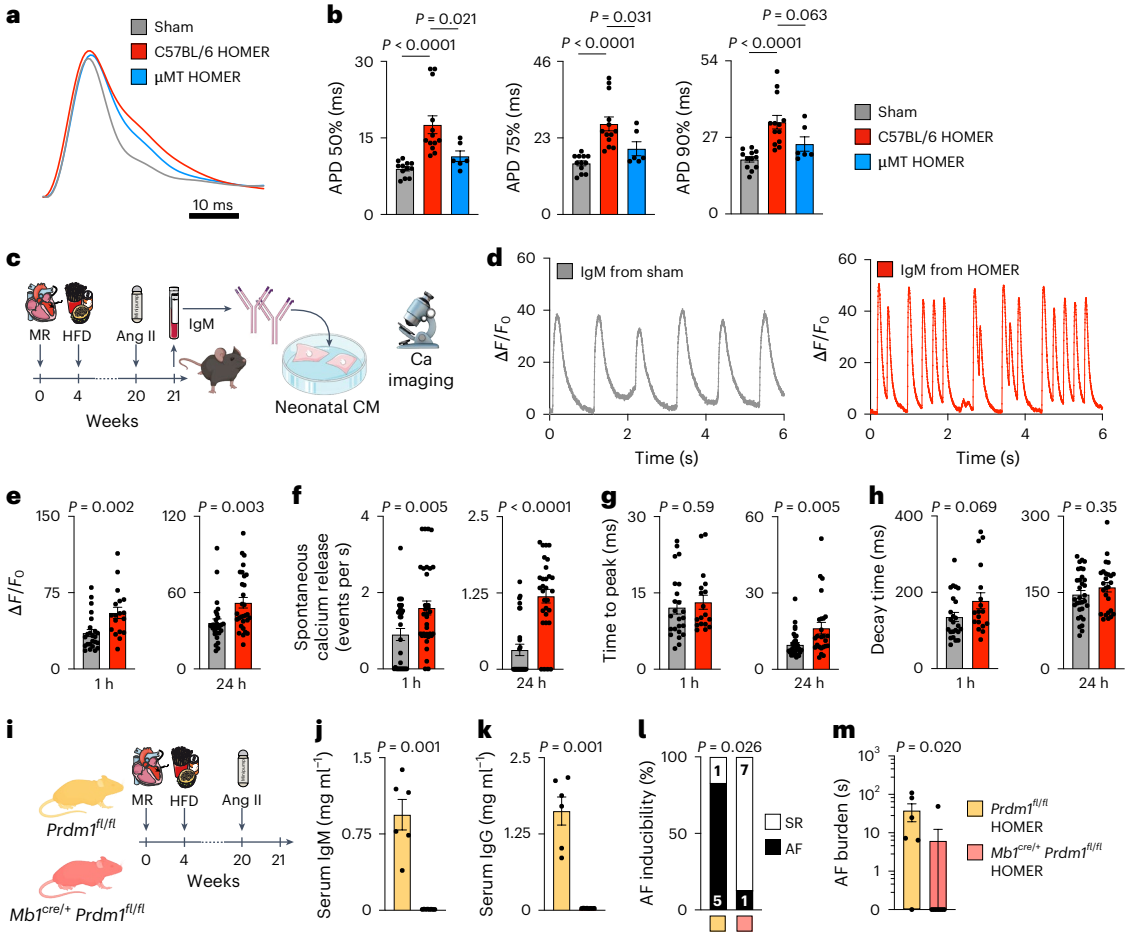

Fig. 6 | IgM isolated from HOMER mice disrupts calcium handling in cardiomyocytes. a, Representative action potential duration in left atria from sham, C57BL/6 HOMER and µMT HOMER mice. **b**, Quantification of action potential duration (APD) 50%, 75% and 90% in left atria from sham, C57BL/6 HOMER and µMT HOMER mice. $n = 12$, $n = 13$ and $n = 6$ per group. **c**, Experimental outline for calcium transient assay: IgM extracted from sham and HOMER serum was applied to mouse neonatal ventricular cardiomyocytes for 1 or 24 h. Fluo-4 dye was used as calcium indicator. **d**, Representative calcium transient in cardiomyocytes incubated with IgM from sham or HOMER mice for 24 h. $\Delta F/F_0$ represents the calcium-related fluorescence changes. **e**–**h**, Parameters of calcium transient in cardiomyocytes incubated with IgM from sham or HOMER mice for 1 h (left) or 24 h (right); amplitude (**e**), spontaneous calcium release events (**f**), time to peak (**g**) and decay time (**h**) are shown (each dot indicates a biological replicate). **i**, Experimental outline: *Mb1*$^{cre/+}$ *Prdm1*$^{fl/fl}$ and *Prdm1*$^{fl/fl}$ littermate controls were subjected to the HOMER protocol. **j**,**k**, Serum levels of IgM (**j**) and IgG (**k**) in *Prdm1*$^{fl/fl}$ and *Mb1*$^{cre/+}$ *Prdm1*$^{fl/fl}$ HOMER mice quantified by ELISA. $n = 6$ and $n = 8$ per group. **l**, Electrophysiological study of AF inducibility in *Prdm1*$^{fl/fl}$ and *Mb1*$^{cre/+}$ *Prdm1*$^{fl/fl}$ HOMER mice. $n = 6$ and $n = 8$ per group. **m**, Electrophysiological study of AF burden in *Prdm1*$^{fl/fl}$ and *Mb1*$^{cre/+}$ *Prdm1*$^{fl/fl}$ HOMER mice. $n = 6$ and $n = 8$ per group. *P* values determined by one-way ANOVA followed by Tukey's multiple comparisons test (**b**), two-tailed Mann–Whitney test (**e**–**h**,**j**,**k**,**m**) or two-sided Fisher's exact test (**l**). Data are the mean ± s.e.m. with individual values for data distribution.

In B cells, the transcription factor BLIMP1 (encoded by *Prdm1*) enables the development of immunoglobulin-producing plasma cells[26]. Thus, *Mb1*$^{cre/+}$ *Prdm1*$^{fl/fl}$ mice have normal B cells but their plasma cell development is arrested[27]. *Mb1*$^{cre/+}$ *Prdm1*$^{fl/fl}$ and *Prdm1*$^{fl/fl}$ control mice were exposed to the HOMER protocol before we evaluated AF inducibility (Fig. 6i). Blood pressure and left atrial fibrosis were similar between both cohorts (Extended Data Fig. 6d–f). *Mb1*$^{cre/+}$ *Prdm1*$^{fl/fl}$ mice that, as expected, had reduced serum immunoglobulin at both baseline (Extended Data Fig. 9g,h) and after HOMER procedures (Fig. 6j,k), exhibited significantly reduced AF inducibility and burden (Fig. 6l,m). Optical mapping of left atria in isolated hearts from *Mb1*$^{cre/+}$ *Prdm1*$^{fl/fl}$ HOMER mice revealed shorter action potential durations than in *Prdm1*$^{fl/fl}$ HOMER control mice (Extended Data Fig. 9i). From these results, we conclude that plasma cell-derived immunoglobulins, particularly IgM, increase inducible AF in HOMER mice. The data obtained in *Mb1*$^{cre/+}$ *Prdm1*$^{fl/fl}$ HOMER mice also address specificity concerns associated with µMT mice, which had shown alterations of various leukocyte classes in absence of B cells.

Proarrhythmic IgM binds the β_1-adrenergic receptor

We next wondered which antigen the increased IgM in HOMER mice binds to. To estimate the molecular weight of proteins to which HOMER IgM bind, we isolated cellular membrane proteins from hearts of µMT mice and immunoblotted those with sera from either HOMER or sham control mice. We detected bands that were absent in no-serum and sham-serum controls, consistent with the presence of several self-antigens targeted by IgM from HOMER mice. Among these, a consistent band was a 50–60-kDa protein (Fig. 7a), which corresponds to the molecular mass of the β_1-adrenergic receptor (also known as ADRB1). This autoantigen would align with our calcium transient data and the increased serum anti-ADRB1 autoantibody titers we measured in individuals with AF (Supplementary Table 2). Underlying comorbidities, which are not matched between shown patient groups, probably contributed to diverging anti-ADRB1 autoantibody levels (Supplementary Table 2). An association between AF and circulating anti-ADRB1 autoantibodies has previously been reported in clinical cohorts[12,13,28,29]. Anti-ADRB1 autoantibodies prolong the action

https://doi.org/10.1038/s44161-025-00724-z

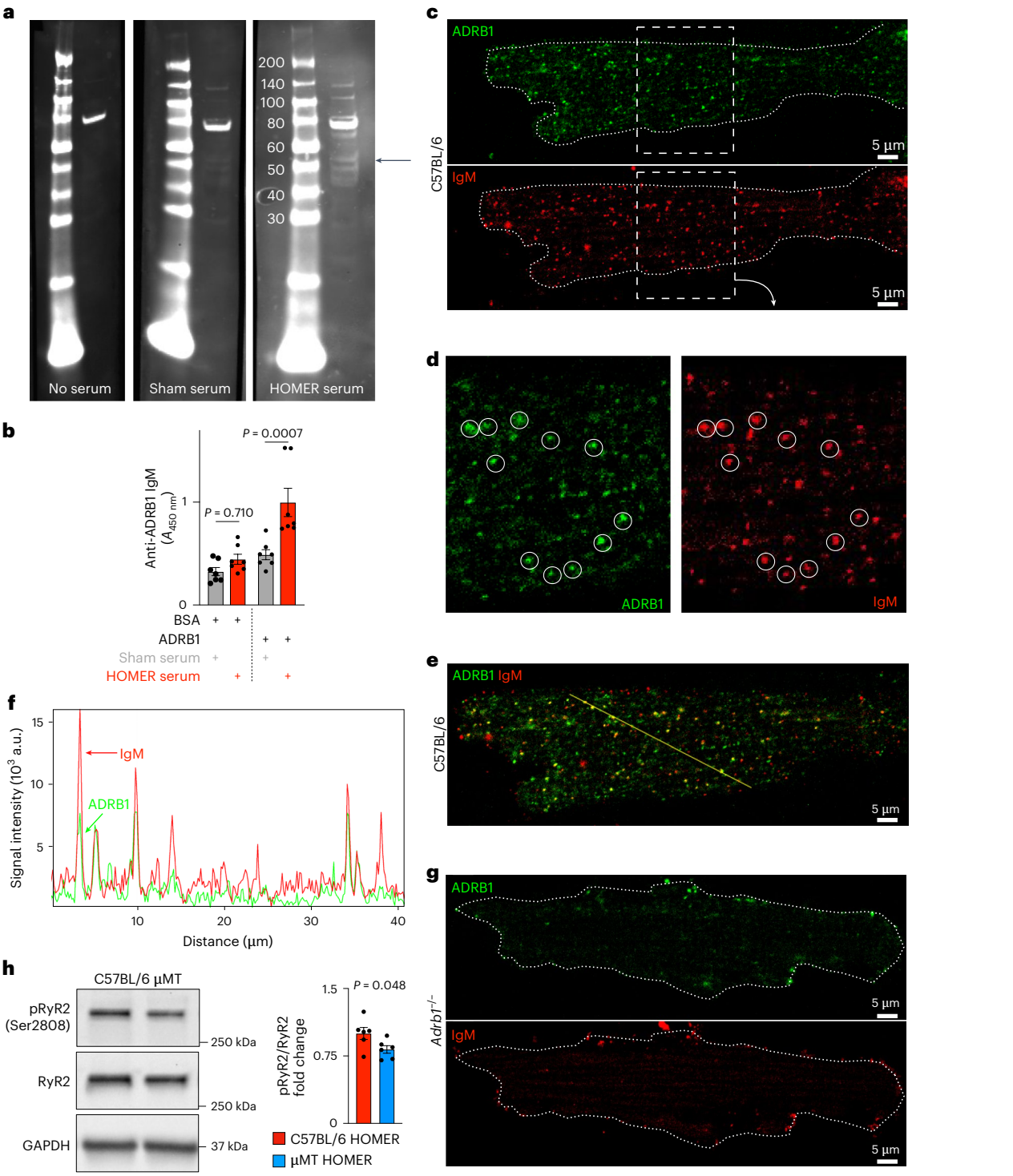

Fig. 7 | HOMER mice develop anti-ADRB1 IgM. a, Immunoblotting image of serum IgM binding protein to cellular membrane proteins of µMT hearts (no serum (left), sham mouse serum (middle) and HOMER mouse serum (right)). Arrow indicates the 50–60-kDa band, which is in the range of the ADRB1 molecular mass. Representative blots are shown for sera from three HOMER and two sham control mice. **b**, IgM titers specific for ADRB1 determined in the serum of sham and HOMER mice by ELISA. $n = 7$ per group. **c**, Representative double staining for ADRB1 (top, green) and IgM (bottom, red) in cardiomyocytes isolated from adult C57BL/6 mice. **d**, Higher magnification of the boxed area indicated in **c** for ADRB1 (left) and IgM (right) staining. Circles indicate signal colocalization of ADRB1 and IgM. **e**, Overlay of ADRB1 and IgM signal in a cardiomyocyte isolated from an adult C57BL/6 mouse. **f**, Signal value of ADRB1 (green) and IgM (red) on the line scan indicated in **e**. **g**, Representative staining of ADRB1 (top, green) and IgM (bottom, red) in cardiomyocytes isolated from adult *Adrb1*$^{-/-}$ mice. Representative stainings are shown for sera from three HOMER mice. **h**, Western blot showing p2808 RyR2 and total RyR2 protein expression in left atrial tissues from C57BL/6 HOMER and µMT HOMER mice. $n = 6$ per group. *P* values determined by one-way ANOVA followed by Tukey's multiple comparisons test (**b**) or two-tailed Student's *t*-test (**h**). Data are the mean ± s.e.m. with individual values for data distribution.

potential duration in atrial cardiomyocytes isolated from individuals with cardiomyopathy[30], matching the prolonged action potential duration in HOMER atria, which was shortened by B cell depletion, as described above (Fig. 6a,b). Therefore, we next examined anti-ADRB1 IgM levels in sham and HOMER sera. Using an enzyme-linked immunosorbent assay (ELISA), we found that HOMER mice had significantly heightened levels of anti-ADRB1 IgM compared with sham mice, whereas nonspecific albumin-binding IgM levels did not differ (Fig. 7b). To validate the finding that HOMER IgM binds to ADRB1, we applied purified IgM from HOMER mice to adult C57BL/6 and *Adrb1*$^{-/-}$ cardiomyocytes, followed by immunofluorescent staining for ADRB1 and IgM. On cardiomyocytes from C57BL/6 mice, immunofluorescent staining of ADRB1 and IgM colocalized (Fig. 7c,d). An intensity plot derived from line scanning supported colocalization of this receptor with deposited IgM (Fig. 7e,f). Manders' correlation coefficient analysis[31] revealed that 63% of IgM fraction overlapped with ADRB1 signal (coefficient, $r = 0.415$). When we repeated costaining for ADRB1 and IgM after incubation with cardiomyocytes isolated from *Adrb1*$^{-/-}$ mice, the IgM signal was much lower (Fig. 7g). We also found that IgG purified from mice 4 weeks after completion of the HOMER protocol can bind ADRB1 (Extended Data Fig. 10a,b).

Furthermore, we assayed protein kinase A (PKA)-mediated cardiac ryanodine receptor (RyR2) phosphorylation, which is downstream of and regulated by ADRB1 stimulation[32]. While left atria from C57BL/6 HOMER mice had higher RyR2 phosphorylation (ratio of pRyR2-Ser2808 to total RyR2) than sham controls (Extended Data Fig. 10c), µMT HOMER mice showed reduced PKA-dependent RyR2 phosphorylation in left atria (Fig. 7h). These observations indicate a lower activation of the ADRB1 signaling cascade in HOMER µMT mice. Decreased phosphorylation of phospholamban (PLN) at Ser16 in HOMER µMT mice further confirmed lower ADRB1-mediated activation of PKA-dependent phosphorylation (Extended Data Fig. 10d).

Our data obtained in HOMER mice, which combine three common AF risk factors, raised questions regarding effects of single risk factor exposure. We began exploring this by atrial flow cytometry analysis for key leukocyte classes and by assaying circulating IgM in mice that were either hypertensive, consumed a high-fat diet or had mitral regurgitation. These pilot studies yielded no significant differences compared to sham controls (Extended Data Fig. 10e,f). A limitation of these data are the potentially underpowered statistics; however, the data motivate further exploration into the synergistic mechanisms that led to autoimmune activity in HOMER mice.

Anti-CD20 monoclonal antibody ameliorates AF inducibility in HOMER mice

Finally, we tested whether B cell depletion with anti-CD20 monoclonal antibodies, a protocol used clinically[33], reduces AF inducibility and burden in HOMER mice. C57BL/6 mice were subjected to HOMER procedures and concomitantly treated with either anti-CD20 antibody or isotype control antibody (Fig. 8a). Anti-CD20 antibody treatment depleted B cells (Fig. 8b), reduced serum levels of IgM and IgG (Fig. 8c,d) and significantly curtailed AF inducibility and burden in HOMER mice (Fig. 8e,f). These findings suggest B cell depletion may be a therapeutic strategy for AF suppression in patients who produce proarrhythmic autoantibodies, especially because this therapy is generally well-tolerated in individuals with rheumatoid arthritis[34].

Discussion

This work describes a humoral immune response in mice exposed to common risk factors for AF. In the HOMER mouse, we reveal (1) how autoimmunity develops after exposure to typical AF risk factors, such as obesity, hypertension and mitral valve regurgitation, and (2) how this contributes to inducible AF. First, while exposed to these risk factors, membrane proteins from stressed or dying cardiomyocytes drain to mediastinal lymph nodes, possibly in DCs. Then, DC-mediated antigen presentation activates and expands autoreactive B cells, which differentiate to plasma cells while exposed to pDC-derived IFNα. Next, plasma cells produce autoantibodies which bind ADRB1 expressed by cardiomyocytes. As a result of ADRB1 binding, PKA activation induces phosphorylation of calcium handling proteins, such as RyR2, which increases calcium-related triggered activity, ultimately promoting AF (Fig. 8g).

Anti-ADRB1 autoantibodies expand in individuals with paroxysmal[13,29] or persistent[28] AF. Because AF creates a vicious cycle (that is AF begets AF)[35], carefully evaluating whether anti-ADRB1 autoantibody expansion is a cause or consequence of AF was warranted. Recently, rabbits immunized with the second loop peptide of ADRB1 showed a higher incidence of inducible AF[29]. Our mechanistic data obtained in µMT HOMER mice after antibody transfer, *Mb1*$^{cre/+}$ *Prdm1*$^{fl/fl}$ HOMER mice and HOMER mice with CD20^{+} B cell depletion provide strong evidence for a causal role of B cell-derived autoantibodies in AF. Our observation that B cells prolong the action potential duration in HOMER atria align with prior reports on anti-ADRB1 autoantibodies in cardiomyopathy[30,36]. Of note, while AF-induced electrical remodeling (which maintains long-standing AF) shortens the action potential duration[37], heterogeneous action potentials may contribute to incipient AF[38], a scenario modeled in the HOMER mouse. Prolonged action potentials are common in mouse AF models, and there are general caveats associated with studying arrhythmia in this species.

Our data indicate that, in HOMER mice, IgM immunoglobulins rose more than IgG. However, we found increased IgG concentrations and ADRB1 binding at later timepoints (4 weeks after completion of the HOMER protocol), indicating that IgG may play a role after AF is established. A plausible explanation for the initial IgM dominance is that expanded plasma cells derive from an extrafollicular response rather than from germinal centers. In accordance with this notion, neither germinal center B cells in mediastinal lymph nodes nor long-lived plasma cells in bone marrow rose in HOMER mice. An extrafollicular B cell response is increasingly appreciated as a dominant mode in autoimmunity. For instance, in both mouse lupus[39] and individuals with systemic lupus erythematosus[40], an extrafollicular B cell response associates with autoantibody production. Intriguingly, pDC-derived IFNα propagates extrafollicular B cell differentiation into short-lived plasma cells that produce autoantibodies[41], and this process aligns with the increased IFNα signaling we observed in HOMER mice. Based on the stronger IgM signal in HOMER mice, we focused on the contribution of IgM to autoantibody-induced AF. However, further studies in humans with AF may explore the relative relevance of IgM and IgG during chronic disease.

In addition to autoantibodies against ADRB1, other autoantigens may contribute to AF. This notion is supported by the additional bands in our immunoblot shown in Fig. 7a. Antibodies against the sodium-potassium pump (Na^+,K^+-ATPase)[42], the M_2 muscarinic receptor[13,28] and potassium channel $K_{ir}3.4$ (ref. 43) have been reported in individuals with AF. High-throughput detection of autoantibodies against precisely folded and embedded membrane proteins, in particular G-protein-coupled receptor proteins, remains challenging; however, future comprehensive autoantibody assays in patients may provide a more detailed catalog of antigens involved in AF pathogenesis. Such antigens may also derive from stromal atrial cells.

In our patient cohort, we cannot determine which factors contributed to lymph node enlargement. That we could not assay DCs, antibody levels and lymph node size in the same patient is another limitation. Beta blockers are frequently used for rate control in individuals with AF[44]. These drugs prevent adrenergic agonist binding but elevate receptor expression[45]. Theoretically, chronic beta blocker use could worsen the pathogenic effect of anti-ADRB1 autoantibodies by upregulating receptors[10], a scenario that would favor combining beta blockade with removal of autoantibodies, if present. Rituximab, a CD20-targeted monoclonal antibody approved for

https://doi.org/10.1038/s44161-025-00724-z

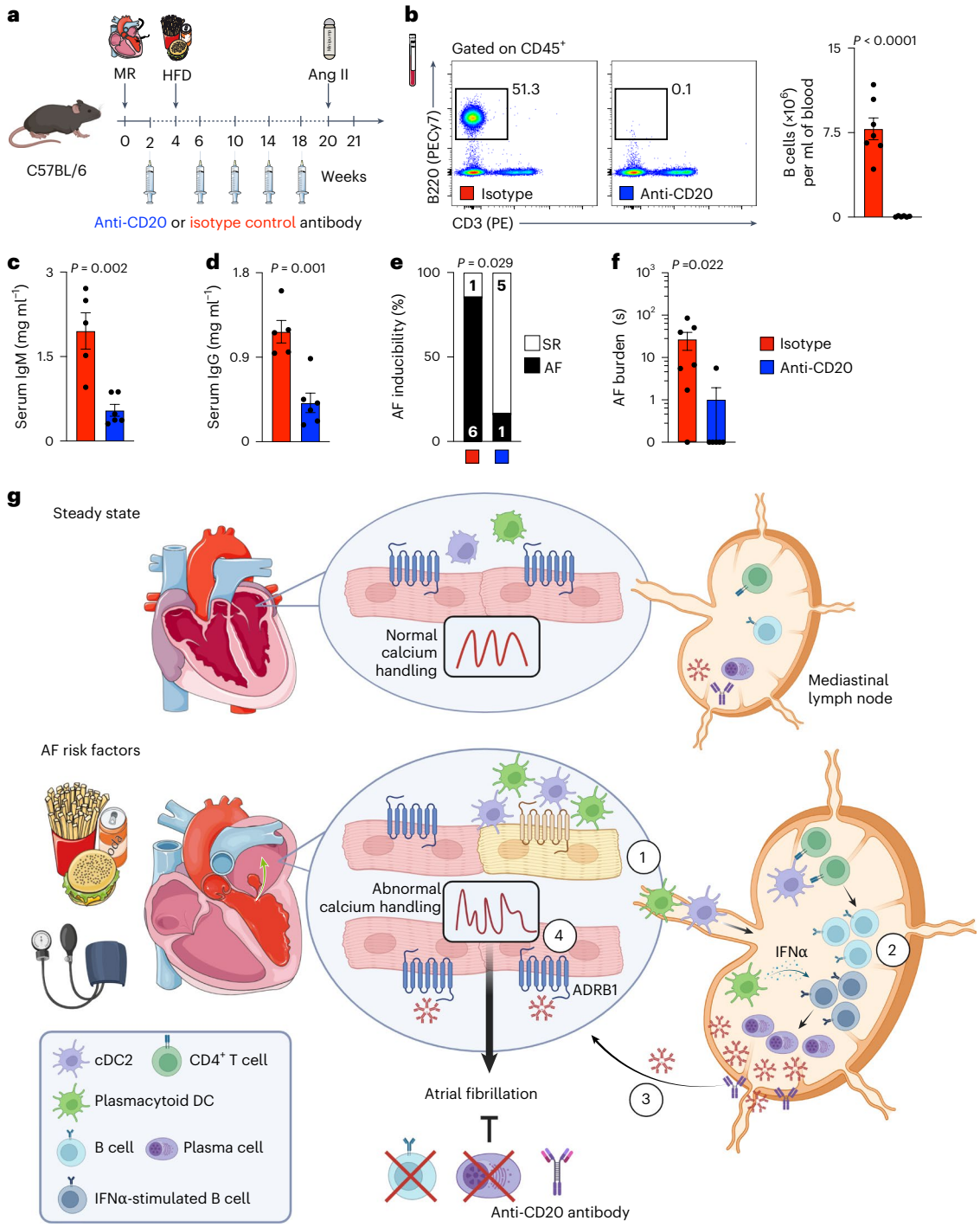

Fig. 8 | Anti-CD20 monoclonal antibody ameliorates AF inducibility. **a**, Experimental outline: anti-CD20 antibody or isotype control antibody was injected into C57BL/6 HOMER mice every 4 weeks. **b**, Flow cytometric quantification of circulating B cells in anti-CD20- or isotype control-treated HOMER mice. $n = 7$ and $n = 6$ per group. **c**,**d**, Serum levels of IgM (**c**) and IgG (**d**) quantified by ELISA in anti-CD20- or isotype control-treated HOMER mice. $n = 5$ and $n = 6$ per group. **e**, Electrophysiological study of AF inducibility in anti-CD20- or isotype control-treated HOMER mice. $n = 7$ and $n = 6$ per group. **f**, Electrophysiological study of AF burden in anti-CD20- or isotype control-treated HOMER mice. $n = 7$ and $n = 6$ per group. *P* values determined by two-tailed Student's *t*-test (**b**–**d**), two-sided Fisher's exact test (**e**) or two-tailed Mann–Whitney test (**f**). Data are the mean ± s.e.m. with individual values for data distribution. **g**, Summary cartoon. Exposure to AF risk factors such as obesity, hypertension and mitral valve regurgitation contributes to AF as follows: (1) activated DCs drain membrane proteins from stressed or dying cardiomyocytes to mediastinal lymph nodes; (2) DC-mediated antigen presentation activates and expands autoreactive B cells, which differentiate to plasma cells while exposed to pDC-derived IFNα; (3) plasma cells produce autoantibodies, which bind ADRB1 expressed by cardiomyocytes; and (4) PKA activation after ADRB1 binding induces phosphorylation of calcium handling proteins, which increases calcium-related triggered activity promoting AF. Please note that the depiction of T cells in the summary cartoon is based on prior studies in other settings rather than own data.

B cell-related cancers, is increasingly used for autoimmune diseases[46]. Notably, safety data for rituximab use in cardiovascular disease are accumulating[47,48]. CD20 cell depletion affects a broad range of antibodies[49]. Aptamer-mediated neutralization of autoantibodies may be a useful strategy without potential for immunodeficiency. Indeed, aptamers for anti-ADRB1 autoantibodies achieved in vivo neutralization in rats[50]. Such an aptamer is under investigation for anti-ADRB1 autoantibody removal in patients with heart failure (ClinicalTrials.gov no. NCT04192214). Considering the clinical implications of our work, a larger patient trial is needed to study whether autoantibody involvement occurs in a specific patient subpopulation, because AF arises from multiple causes and diverse risk factors.

In summary, B cells promote adverse electrical remodeling and elicit AF through proarrhythmic autoantibody production in mice with mitral valve regurgitation, obesity and hypertension. Our data indicate that humoral immunity may be a treatment target for certain forms of AF.

Methods

Human samples

Analysis of thoracic lymph node size was undertaken as a substudy from the Oxford Risk Factors And Non-Invasive Imaging (ORFAN) Study (ethics committee reference 15/SC/0545, Confidentiality Advisory Group reference 20/CAG/0157). A cohort of age- and sex-matched patients with AF or sinus rhythm undergoing coronary computed tomography (CCTA) were randomly identified from the registry arm of the ORFAN study. Patients underwent CCTA according to the protocol at the respective site but typically included a >64-slice scanner. Between 60 and 80 ml, iodine-based contrast medium (Niopam 370, Bracco Imaging) was typically given at a flow rate of 5–7 ml s^{-1} (tube energy of 100 or 120 kVp, axial slice thickness of 0.5 mm, tube rotation 0.25 s). Standard CCTA reconstruction algorithm was used to generate the images at 75% phase of the cardiac cycle. An expert analyst blinded to heart rhythm status conducted manual segmentation of thoracic lymph nodes according to the IASLC lymph node map 2009 and other structures using Slicer v5.2.2 software. All visible nodes within the mediastinum were contoured in multiple sequential two-dimensional axial slices, cross referenced in coronal slices, to derive individual node volumes.

To explore the prevalence of anti-ADRB1 in humans with and without AF, stored frozen plasma samples were randomly selected from patients who had participated in one of two ethically approved clinical trials; all patients freely gave their written informed consent. For the sinus rhythm group, samples were selected at random from patients (n = 152) who participated in the Statin Therapy in Cardiac Surgery (STICS) trial (ClinicalTrials.gov no. NCT01573143, the methodology and primary results of STICS have been published previously[51]). All patients in this trial were confirmed by electrocardiogram (ECG) to be in sinus rhythm at the time this sample was taken (baseline sample, before planned cardiac surgery and before trial group allocation). For the AF group, samples were selected at random from patients (n = 41) participating in the LOSE-AF trial (ClinicalTrials.gov no. NCT03713775). All patients were confirmed by ECG to be in AF at the time this baseline sample was acquired. While known risk factors for AF were present in patients in both trials, the inclusion/exclusion criteria differed, and patients in LOSE-AF were required to have elevated body mass index to enter the study. No matching for baseline characteristics was attempted, and key baseline characteristics are presented in Supplementary Table 2. Anti-ADRB1 autoantibodies were measured using a commercially available ELISA, which detects IgG and IgM against anti-ADRB1 (Abbexa). The assay was performed at a central core laboratory (University of Oxford Nuffield Department of Population Health Clarendon Laboratory) and automated using a Beckman Coulter i7 liquid handling system with integrated 405LS plate washer (BioTek), Cytomat 2 incubator (Thermoscientific) and SpectraMax iD3 plate reader (Molecular Devices). Anti-ADRB1 autoantibody status was considered positive if the assay indicated a titer higher than the minimum reliable detection limit of 6.25 ng ml^{-1}, and negative if below this or undetectable.

Mice

Wild-type C57BL/6 (stock 000664); B6.129S2-*Ighm*^{tm1Cgn}/J (μMT, stock 002288); B6.C(Cg)-Cd79a$^{tm1(cre)Reth}$/EhobJ (*Mb1*^{Cre}, stock 020505); B6.129-*Prdm1*^{tm1Clme}/J (*Prdm1*$^{fl/+}$, stock 008100); B6.FVB-Tg (*Myh6*-cre) 2182Mds/J (*Myh6*^{Cre}, stock 011038); Gt (ROSA) 26Sor$^{tm4(ACTB-tdTomato,-EGFP)Luo}$/J (*mTmG*$^{fl/+}$, stock 007576); B6.FVB-1700016L21Rik$^{Tg(Itgax-HBEGF/EGFP)57Lan}$/J (*Cd11c*^{DTR}, stock 004509), B6.129S2-H2$^{dlAb1-Ea}$/J (MHCII$^{-/-}$, stock 003584) and *Adrb1*^{tm1Bkk} *Adrb2*^{tm1Bkk}/J (*Adrb1*$^{-/-}$, stock 003810) were purchased from Jackson Laboratory. Genotyping for each strain was performed as described on the Jackson Laboratory website. All experiments were performed with 8- to 12-week-old male animals and using age-matched groups. Where appropriate, mice were randomly assigned to interventions. All mice were group-housed under standard conditions with free access to food and water. All animal experiments were approved by the Institutional Animal Care and Use Committee at the Massachusetts General Hospital (protocol no. 2014N000078).

HOMER model

We used our HOMER mouse model to model AF in vivo. The HOMER model, described in detail elsewhere, was created to induce atrial remodeling and a disease condition that combines three clinical risk factors for AF[5]. In brief, mice first underwent either sham surgery or surgery to generate mitral valve regurgitation. The mice were anesthetized (2.5% isoflurane in 95% O_2), intubated, ventilated and placed on a heating pad. After rotating the mouse to the right, a left lateral thoracotomy (second intercostal space) was performed and the pericardium was opened. The left atrium was elevated, and a 8.0 suture was inserted into the inferior part of the left atrium just above the mitral annulus. The needle was guided through the posterior leaflet of the mitral valve without visual control and exerted through the left ventricle just inferior of the mitral annulus and superior to the left circumflex artery. A surgical knot was performed to snare the posterior leaflet of the mitral valve to the left ventricular wall. The intercostal space and skin were surgically closed and the mouse was allowed to recover with oxygen on a heating pad until extubation. For sham surgery, mice underwent left thoracotomy as described above, and the pericardium was incised[5]. Four weeks after surgery, either normal chow or high-fat diet (Research Diets, D12492) was initiated and continued for 17 weeks. Finally, 20 weeks after mitral valve surgery, mice were exposed to continuous infusion of either saline or angiotensin II (1 μg kg^{-1} min^{-1}) for 1 week via a subcutaneously implanted osmotic pump.

B cell depletion with anti-CD20 monoclonal antibody

A total of 2 weeks after mitral valve surgery, randomized grouped mice were intravenously injected every 4 weeks with 250 μg of sterile anti-mouse CD20 antibody (BioLegend, clone SA271G2) or isotype control (rat IgG2b, BioLegend, clone RTK4530).

Electrophysiological study

Electrophysiological studies were performed as perviously described[5]. A Millar EPR-800 octapolar catheter was inserted into the right jugular vein and positioned in the right atrium and ventricle. Arrhythmia induction was performed with double extrastimuli (S1–S2–S3) at two S1 cycle lengths (120 and 100 ms), progressively decreasing S2 and S3 to 10 ms, as well as burst pacing, and each set of stimulation was done twice. Burst pacing was done at a duration of 3 s and then 6 s, with cycle length starting at 50 ms and progressing to 10 ms in intervals of 5 ms. AF was defined as irregular ventricular response with rapid atrial rhythm. The mice were considered inducible if they had at least one episode of AF longer than 1 s. The total AF burden for any given mouse

was obtained by summing all episodes of AF >250 ms during the course of the entire electrophysiological study.

Optical mapping

Isolation and perfusion of the heart were performed as previously described[52]. In brief, the mouse was anesthetized using isoflurane and the heart was excised and perfused via an aortic cannula. The cannulated heart was then perfused with a modified Tyrode's solution (128.2 mM NaCl, 4.7 mM KCl, 1.19 mM NaH_2PO_4, 1.05 mM $MgCl_2$, 1.3 mM $CaCl_2$, 20.0 mM $NaHCO_3$, 11.1 mM glucose; pH 7.35 ± 0.05) using a Langendorff perfusion setup. Blebbistatin (10 mM, Tocris Bioscience, Bio-Techne) was used to arrest cardiac motion. The heart was stained for 30 min with a voltage-sensitive dye (di-4-ANEPPS, 2 mmol l^{-1} in dimethyl sulfoxide, Invitrogen). Custom-made epicardial platinum electrodes and a Medtronic stimulator were used to pace the heart. Pacing was performed at 60 to 120 ms cycle lengths (4 ms square wave stimuli). A halogen light source (X-Cite, 150 W, filtered at 520 ± 45 nm) was used to excite fluorescence. Emissions greater than 610 nm were collected and focused onto an 80 × 80 charge-coupled device camera (RedShirtImaging SMQ Camera and Macroscope IIA) using a 50 mm original magnification ×2.7 lens. The data sampling was performed at 2,000 frames per second with a filter setting of 1 kHz. A specifically designed Matlab program was used to analyze data in order to generate action potential durations at 50%, 70% and 90% repolarization.

Blood pressure measurements

Blood pressure in conscious mice was measured with a noninvasive tail cuff system (Kent Scientific Corporation). The systolic and diastolic blood pressures were obtained by averaging five measurements per animal.

IgM purification

IgM were purified from sham and HOMER mice sera using an IgM Purification kit (Pierce Biotechnology). The IgM containing elution was concentrated and dialyzed using an Amicon Ultra-15 Centrifugal Filter device (Millipore). The concentrate was diluted with normal saline and filtered to obtain a sterile antibody solution. For the calcium and immunocytochemistry assay, IgM was used at a final concentration of 2 µg ml^{-1}. For the in vivo transfer assay, 120 µg of IgM diluted in 200 µl of saline was passively transferred into µMT HOMER mice via intraperitoneally injections 2 days before the electrophysiological study[53].

IgG purification

IgG were purified from sham and HOMER mice sera using an IgG Purification kit (Thermo Fisher). The IgG containing elution was analyzed using ELISA. The concentrate was diluted with normal saline and filtered to obtain a sterile antibody solution. For the immunocytochemistry assay, IgG was used at a final concentration of 2 µg ml^{-1}.

Calcium assay

Neonatal mouse cardiomyocytes were isolated by enzymatic digestion. The 1- to 2-day-old pups were killed, the hearts were removed and the ventricles were collected. The tissues were dissociated in Hanks' balanced salt solution (HBSS) containing 0.1% trypsin (Sigma-Aldrich) overnight at 4 °C under agitation, followed by three consecutive digestion steps in HBSS containing 335 U ml^{-1} collagenase II (Worthington Biochemical Corporation) for 2 min at 37 °C with gentle agitation. The digest was filtered through a 40-µm nylon mesh, washed and resuspended in culture medium. The cell suspensions were preplated into 100-mm cell culture dishes and incubated at 37 °C for 45 min to allow attachment of nonmyocyte cell populations and enrichment of the cardiomyocyte population. Cardiac cells remaining in suspension were collected and seeded on 8-mm coverslips coated with fibronectin (Sigma-Aldrich). On day 4, cardiomyocytes were loaded with fluo-4 NW (ThermoFisher Scientific) in normal Tyrode's solution for 45 min at room temperature. Fluo-4 fluorescence was obtained with a FITC filter set (excitation: HQ480, mirror: Q505LP, emision: HQ535/50 m; Chroma) and an X-cite exact mercury arc lamp (Lumen Dynamics) with a 50% output for illumination. Fluorescent images with or without pacing stimulation (1 Hz) were recorded using a Nikon Eclipse Ti-U inverted microscope (Nikon Instruments), a NeuroCCDSM camera (RedShirtImaging) and the Neuroplex software (RedShirtImaging). Intracellular calcium transients were analyzed with Neuroplex and Clampfit v9.2 (Molecular Devices). Cyclic calcium transients were analyzed to determine amplitude, time to peak and transient decay time with a monoexponential fit[54]. Adult atrial cardiomyocyte calcium measurements were performed as previously described[55]. For cardiomyocyte isolation, the aorta was clamped, the heart excised and antegradely perfused by a needle in the left ventricle. Enzymatic digestion was performed by collagenase and proteinase. After enzymatic digestion, the atrium was dissected and cardiomyocytes were mechanically isolated before calcium was reintroduced to the cell suspension[56]. Isolated atrial cardiomyocytes were loaded with the Ca^{2+} indicator Fluo 4-AM (10 µmol l^{-1} for 15 min, Molecular Probes) at room temperature. The solution was substituted and cells were incubated for 15 min with Tyrode's solution. Line scans for Ca^{2+} measurements were obtained with a laser scanning confocal microscope. Line scans were recorded during systole with continuous field stimulation at 1 Hz and during diastole. Ca^{2+} transients were analyzed with the program LabChart (ADInstruments).

Immunocytochemistry assay

Adult mouse ventricular cardiomyocytes were isolated using a Langendorff-free method as described previously[56]. In brief, C57BL/6 or *Adrb1*$^{-/-}$ mice were anesthetized with isoflurane, and the heart was exposed and immediately flushed by injecting ethylenediaminetetraacetic acid (EDTA) buffer directly into the right ventricle. Next, the heart was excised and digested by injection of EDTA buffer and perfusion buffer followed by prewarmed digestion buffer (collagenase 2, collagenase 4 and protease XI) into the left ventricle. Once cellular dissociation had been completed by gentle trituration, a stop buffer solution was added. After passing through a 250-µm filter, cells underwent sequential rounds of gravity settling to obtain a highly pure cardiomyocytes fraction and were resuspended with perfusion buffer containing gradually increased Ca^{2+} concentration from 0.012 to 1.2 mM. Single cardiomyocytes were seeded onto 8-mm coverslips precoated with fibronectin and incubated at 37 °C in a 5% CO_2 incubator. After 45 min of incubation, the cells were fixed with 4% paraformaldehyde for 10 min at room temperature followed by washing with PBS and blocking with 10% donkey serum, 5% goat serum and 1% bovine serum albumin (BSA) in PBS-T (0.1% Tween-20) for 1 h at room temperature. The cells were stained with rabbit anti-ADRB1 (1:400, Alomone Labs) and purified HOMER IgM or IgG diluted in 1% BSA PBS-T at 4 °C overnight. For indicated experiments HOMER IgM and IgG concentrations were matched to the concentration of sham controls. After washing, the cells were stained with donkey anti-rabbit Alexa Fluor 647 (1:1,000, ThermoFisher Scientific) and goat anti-mouse Alexa Fluor 568 (1:1,000, ThermoFisher Scientific) at room temperature for 1 h while protected from light. The cells were imaged with a confocal microscopy (Zeiss LSM800 Airyscan) at 40× magnification. The images were analyzed with ImageJ software (National Institutes of Health).

Tissue processing and cell collection

Mouse peripheral blood was collected by retro-orbital bleeding using heparinized capillary tubes, and red blood cells were lysed with 1× red blood cell lysis buffer (BioLegend). For organ collection, an incision was made in the right atrium and mice were perfused through the left ventricle with 10 ml of ice-cold PBS. Mediastinal and iliac lymph nodes were carefully excised using a dissection microscope. Lymph nodes were then plunged and filtered through a 40-µm cell strainer. For analysis of the bone marrow, the epiphyses of the tibia were carefully

opened and flushed with FACS buffer (1× PBS supplemented with 0.5% BSA). The collected bone marrow cells were then filtered through a 40-µm cell trainer. Left atrial tissues were excised using a dissection microscope, minced into small pieces and enzymatically digested with 450 U ml^{-1} collagenase I, 125 U ml^{-1} collagenase XI, 60 U ml^{-1} DNase I and 60 U ml^{-1} hyaluronidase (all Sigma-Aldrich) for 30 min at 37 °C under agitation. After digestion, the tissues were washed and filtered through a 40-µm cell strainer and subsequently centrifuged to obtain single-cell suspensions.

Flow cytometry

To detect leukocyte subsets, cell suspensions were stained for 30 min at 4 °C in FACS buffer. For analysis of blood leukocytes, cells were stained with CD45 (BioLegend, clone 30-F11); CD11b (BioLegend, clone M1/70); Ly6G (BioLegend, clone 1A8); CD3 (BioLegend, clone 17A2); B220 (BioLegend, clone RA3-6B2); CD19 (BioLegend, clone 6D5); CD115 (BioLegend, clone AFS98); and Ly6C (BioLegend, clone HK1.4). For analysis of tissue DCs, the cells were stained with CD45 (BioLegend, clone 30-F11); CD19 (BioLegend, clone 6D5); CD11b (BioLegend, clone M1/70); CD11c (BioLegend, clone N418); MHCII (BioLegend, clone M5/114.15.2); CD3 (BioLegend, clone 17A2); Ly6G (BioLegend, clone 1A8); NK1.1 (BioLegend, clone PK136); CD64 (BioLegend, clone X54-5/7.1); CD317 (BioLegend, clone 551/927); CD80 (BioLegend, clone 16-10A1); and XCR1 (BioLegend, clone ZET). For analysis of tissue T cells, B cells and plasma cells, cells were stained with B220 (BioLegend, clone RA3-6B2); GL7 (BioLegend, clone GL7); Fas (BioLegend, clone SA367H8); CD3 (BioLegend, clone 17A2); CD4 (BioLegend, clone GK1.5); CXCR5 (BioLegend, clone L138D7); CD138 (BioLegend, clone 281-2); TACI (BioLegend, clone 8F10); CD23 (BioLegend, clone B3B4), CD21/CD35 (BioLegend, clone 7E9), IgD (BioLegend, clone 11-26 c.2a) and IgG (BioLegend, clone RMG1-1). DAPI or LIVE/DEAD Fixable Aqua Dead Cell Stain (Life Technologies) was used as a cell viability marker. To control for potential confounders of atrial digestion protocols for flow cytometric cell quantification, we included sham-operated controls in every experiment. The data were acquired on a BD FASAria II, BD LSRII flow cytometer or Attune NxT flow cytometer (ThermoFisher Scientific) and analyzed with FlowJo v10 software.

Flow cytometry gating

Blood B cells were gated as CD19$^+$ B220$^+$ CD3$^-$, T cells as CD19$^-$ B220$^-$ CD3$^+$, neutrophils as CD19$^-$ B220$^-$ CD3$^-$ CD11b$^+$ CD115$^{low/int}$ Ly6G$^+$ and monocytes as CD19$^-$ B220$^-$ CD3$^-$ CD11b$^+$ CD115^{high} Ly6G$^-$ Ly6C$^{low/high}$. Tissue pDC were gated as CD45$^+$ CD19$^-$ CD3$^-$ Ly6G$^-$ NK1.1$^-$ CD11c^{int} CD317$^+$, cDC1 as CD45$^+$ CD19$^-$ CD3$^-$ Ly6G$^-$ NK1.1$^-$ CD317$^-$ CD11c$^+$ MHCII$^+$ XCR1$^+$ and cDC2 as CD45$^+$ CD19$^-$ CD3$^-$ Ly6G$^-$ NK1.1$^-$ CD317$^-$ CD11c$^+$ MHCII$^+$ CD11b$^+$ (ref. 57). Tissue B cells were gated as B220$^+$, germinal center B cells as B220$^+$ GL7$^+$ Fas$^+$, follicular helper T cells as CD3$^+$ CD4$^+$ PD1$^+$ CXCR15$^+$ (ref. 58), plasma cells as CD138$^+$ TACI$^+$ (ref. 59), age-associated B cells as CD23$^-$ CD21$^-$ CD35$^-$, follicular B cells as CD23$^+$ CD21$^+$ CD35$^+$, plasmablasts as CD138$^+$ B220$^+$ CD19$^+$, naive B cells as IgG$^-$ IgD$^+$ and class-switched activated B cells as IgG$^+$ IgD$^-$.

Antigen immunoblotting assay

Plasma membrane proteins were selectively extracted from µMT mice hearts using the Plasma Membrane Protein Extraction kit (Abcam) according to the manufacturer's instructions. After measuring the protein concentration with a BCA assay, 20 µg of membrane proteins were subjected to electrophoresis using the NuPAGE 4–12% Bis–Tris protein gel (ThermoFisher Scientific) and were blotted to a nitrocellulose membrane using the iBlot Gel transfer system (ThermoFisher Scientific). The membrane was blocked with Intercept blocking buffer (LI-COR) for 1 h at room temperature. Each lane of the membrane was then stained with sham or HOMER serum (1:200) in blocking buffer overnight at 4 °C with gentle agitation. After washing, the membrane was stained with IRDye 800CW goat anti-mouse IgM (1:2500, LI-COR) in blocking buffer for 30 min at room temperature. After washing, the signal was visualized using an Azure Biosystems Sapphire Biomolecular imager and analyzed with ImageJ.

Western blotting

The total protein was extracted from left atria tissue in RIPA lysis buffer supplemented with a protease/phosphatase inhibitor cocktail (Roche). The protein concentration was measured using a BCA assay. Lysates of 20 µg were subjected to electrophoresis using the 4–15% protein gel (Bio-Rad) and blotted to a nitrocellulose membrane using the Trans-Blot Turbo transfer system (Bio-Rad). Anti-p2808 RyR2 antibody (1:1,000, Badrilla, A010-30), anti-RyR2 antibody (1:15,000, ThermoFisher, PA5-87416), anti-GAPDH antibody (1:5,000, Cell Signaling, 2118), anti-phospholamban Ser16 (1:1,000, ThermoFisher, PA5-117226), anti-phospholamban (1:1,000, ThemoFisher, PA5-119803) and HRP-conjugated secondary antibodies (1:5,000, Cell Signaling, 7074) were used. The signals were visualized with chemiluminescent substrate (ThermoFisher Scientific, PI34578) and densitometric analysis was performed with Image Lab software (Bio-Rad).

ELISA

INFα levels and total IgM and IgG levels in mouse serum samples were quantified by ELISA according to the manufacturer's protocol (PBL assay science and Bethyl Laboratories, respectively). Mouse anti-ADRB1 antibodies were measured as follows: 96-well Nunc MaxiSorp plates (ThermoFisher Scientific) were coated with mouse recombinant ADRB1 protein (2 µg ml^{-1}, Cusabio) in PBS. After overnight incubation at 4 °C, plates were washed and blocked in 2% BSA in PBS-T and incubated for 1 h at room temperature. Serum samples were added at 1:100 (IgM) or 1:200 (IgG) dilutions and incubated for 2 h at 37 °C. After washing, HRP-conjugated goat anti-mouse IgM (1:10,000, Abcam) or IgG (1:10,000, Abcam) was added and incubated for 1 h at 37 °C. The samples were developed using 3,3′,5,5′-tetramethylbenzidine (TMB) substrate solution (ThermoFisher Scientific) according to the manufacturer's instructions. The reaction was stopped with stop solution (ThermoFisher Scientific) and the absorbance was measured with a plate reader at 450 nm.

Real-time qPCR

Total RNA from mediastinal lymph nodes was extracted using the RNeasy Micro kit (Qiagen) according to the manufacturer's protocol. High-Capacity RNA-to-cDNA kit (ThermoFisher Scientific) was used for reverse transcription. PowerUp SYBR Green Master Mix (ThermoFisher Scientific) and primers for *Infa* (forward: AGCCTGTGTGATGCAGGAACC, reverse: CAGCAAGTTGGTTGAGGAAGAG) and *Gapdh* (forward: TGTGATGGGTGTGAACCACGAGAA, reverse: GAGCCCTTCCACAATGCCAAAGTT) were used to quantify gene expression. The fold changes were normalized to *Gapdh* mRNA using the $2^{-\Delta\Delta Ct}$ method.

Histology

The mouse hearts were collected and embedded in OCT compound (Sakura Finetek). Fresh-frozen serial sections (7-µm thickness) were prepared and fixed with 4% paraformaldehyde for 10 min at room temperature. The tissue sections were blocked with Carbo-free working solution (Vector Laboratories) for 30 min at room temperature and then incubated with sham or HOMER mice serum diluted in blocking buffer (1:20) for 1 h at room temperature. After PBS washes, the sections were incubated with Alexa Fluor 555 goat anti-mouse IgM (1:100, ThermoFisher Scientific) for 30 min at room temperature followed by staining with WGA Alexa Fluor 488 (1:100, ThermoFisher Scientific) and anti-cardiac troponin I antibody (1:200, Abcam). Troponin I was detected by goat anti-rabbit IgG (H + L) Alexa Fluor 488 secondary antibody (1:100, ThermoFisher Scientific), and the sections were counterstained with DAPI (1:3,000, ThermoFisher Scientific). To detect atrial fibrosis, sections were fixed with 10% formalin for 30 min at

room temperature and incubated in Bouin's fixative solution (Electron Microscopy Sciences) overnight at room temperature. The nuclei were stained with a mixture of Weigert's iron hematoxylin solution A and B (Electron Microscopy Sciences) for 5 min at room temperature. The sections were then stained with Biebrich scarlet-acid fuchsin (StatLab), followed by phosphomolybdic acid/phosphotungstic acid solution (Sigma-Aldrich) and Aniline blue stain (StatLab). All slides were scanned with the NanoZoomer 2.0RS digital slide scanner (Hamamatsu) and analyzed with ImageJ.

Single-cell RNA-seq computational analysis

The single-cell RNA-seq data were analyzed as we described previously[5]. In detail, human and mouse data were processed with Cell Ranger 3.0.2 from 10x Genomics using the GRCh38 and GRCm38 (mm10) reference genome, respectively. Low quality cells were filtered out, which included cells with fewer than 500 unique molecular identifiers, cells expressing fewer than 200 genes or cells in which the mitochondrial genes accounted for over 25% of total unique molecular identifier count. Genes expressed in fewer than three cells were also filtered out. Seurat v3.1 (refs. 60,61) was used to carry out count normalization with sctransform[62], followed by integration[60], which identified shared cell states across the samples. FindMarkers and FindconservedMarkers functions in Seurat were used to identify markers for each cluster to help with the cluster annotations. Pseudobulk differential expression analysis[63] was carried out to detect genes that are differentially expressed between cells with different disease conditions. Aggregating the cells to the sample level, we performed the differential expression analysis using the quasi-likelihood F-test with edgeR v3.34.1 (refs. 64–66). The GSEAPreranked tool from GSEA v4.2.2 (refs. 67,68) was then used to perform the GSEA with the collections of gene sets in the Molecular Signatures Database (MSigDB) 7.5.1 (refs. 67,69). The genes were ranked by their fold-change between disease conditions, which was obtained from the differential expression analysis.

Statistics

The data are shown as mean ± s.e.m. A statistical analysis was performed using GraphPad Prism 9 and Stata 18. Statistical tests included two-sided Fisher's exact tests, two-sided chi-square tests, two-tailed Student's *t*-tests, two-tailed independent groups *t*-tests, two-tailed Mann–Whitney tests (when Gaussian distribution was not assumed) and ANOVA followed by Tukey's multiple comparisons test. The *P* values of 0.05 or less were considered significant. Animal group sizes were as low as possible and empirically chosen.

Reporting summary

Further information on research design is available in the Nature Portfolio Reporting Summary linked to this article.

Data availability

Raw and processed mouse scRNA-seq data as well as processed human scRNA-seq data are available at the NCBI's Gene Expression Omnibus (GEO) database under accession no. GSE224959. Raw human scRNA-seq data are accessible at the controlled access repository Data Use Oversight System (DUOS; https://duos.broadinstitute.org) under accession number DUOS-000150 under the restrictions listed by this system, which is an MGH IRB-approved option that protects patient identity.

References

1. Kornej, J., Börschel, C. S., Benjamin, E. J. & Schnabel, R. B. Epidemiology of atrial fibrillation in the 21st century: novel methods and new insights. *Circ. Res.* **127**, 4–20 (2020).
2. Kim, M. H., Johnston, S. S., Chu, B. C., Dalal, M. R. & Schulman, K. L. Estimation of total incremental health care costs in patients with atrial fibrillation in the United States. *Circ. Cardiovasc. Qual. Outcomes* **4**, 313–320 (2011).
3. Andrade, J. G. et al. Cryoablation or drug therapy for initial treatment of atrial fibrillation. *N. Engl. J. Med.* **384**, 305–315 (2021).
4. Hu, Y.-F., Chen, Y.-J., Lin, Y.-J. & Chen, S.-A. Inflammation and the pathogenesis of atrial fibrillation. *Nat. Rev. Cardiol.* **12**, 230–243 (2015).
5. Hulsmans, M. et al. Recruited macrophages elicit atrial fibrillation. *Science* **381**, 231–239 (2023).
6. Martini, E. et al. Single-cell sequencing of mouse heart immune infiltrate in pressure overload-driven heart failure reveals extent of immune activation. *Circulation* **140**, 2089–2107 (2019).
7. Litviňuková, M. et al. Cells of the adult human heart. *Nature* **588**, 466–472 (2020).
8. Chaffin, M. et al. Single-nucleus profiling of human dilated and hypertrophic cardiomyopathy. *Nature* **608**, 174–180 (2022).
9. Guilliams, M. et al. Unsupervised high-dimensional analysis aligns dendritic cells across tissues and species. *Immunity* **45**, 669–684 (2016).
10. Düngen, H. D. et al. β_1-Adrenoreceptor autoantibodies in heart failure: physiology and therapeutic implications. *Circ. Heart. Fail.* **13**, e006155 (2020).
11. Lazzerini, P. E., Capecchi, P. L., Laghi-Pasini, F. & Boutjdir, M. Autoimmune channelopathies as a novel mechanism in cardiac arrhythmias. *Nat. Rev. Cardiol.* **14**, 521–535 (2017).
12. Stavrakis, S. et al. Activating autoantibodies to the beta-1 adrenergic and M2 muscarinic receptors facilitate atrial fibrillation in patients with Graves' hyperthyroidism. *J. Am. Coll. Cardiol.* **54**, 1309–1316 (2009).
13. Yalcin, M. U. et al. Elevated M2-muscarinic and β1-adrenergic receptor autoantibody levels are associated with paroxysmal atrial fibrillation. *Clin. Res. Cardiol.* **104**, 226–233 (2015).
14. Li, H. et al. Inducible cardiac arrhythmias caused by enhanced β1-adrenergic autoantibody expression in the rabbit. *Am. J. Physiol. Heart. Circ. Physiol.* **306**, H422–H428 (2014).
15. Simmons, D. P. et al. Type I IFN drives a distinctive dendritic cell maturation phenotype that allows continued class II MHC synthesis and antigen processing. *J. Immunol.* **188**, 3116–3126 (2012).
16. Banchereau, J. & Pascual, V. Type I interferon in systemic lupus erythematosus and other autoimmune diseases. *Immunity* **25**, 383–392 (2006).
17. Price, M. J., Patterson, D. G., Scharer, C. D. & Boss, J. M. Progressive upregulation of oxidative metabolism facilitates plasmablast differentiation to a T-independent antigen. *Cell Rep.* **23**, 3152–3159 (2018).
18. Eisenbarth, S. C. Dendritic cell subsets in T cell programming: location dictates function. *Nat. Rev. Immunol.* **19**, 89–103 (2019).
19. Van der Borght, K. et al. Myocardial infarction primes autoreactive T cells through activation of dendritic cells. *Cell Rep.* **18**, 3005–3017 (2017).
20. Jego, G. et al. Plasmacytoid dendritic cells induce plasma cell differentiation through type I interferon and interleukin 6. *Immunity* **19**, 225–234 (2003).
21. De Silva, N. S. & Klein, U. Dynamics of B cells in germinal centres. *Nat. Rev. Immunol.* **15**, 137–148 (2015).
22. Madsen, L. et al. Mice lacking all conventional MHC class II genes. *Proc. Natl Acad. Sci. USA* **96**, 10338–10343 (1999).
23. Jung, S. et al. In vivo depletion of $CD11c^+$ dendritic cells abrogates priming of $CD8^+$ T cells by exogenous cell-associated antigens. *Immunity* **17**, 211–220 (2002).
24. Burstein, B. & Nattel, S. Atrial fibrosis: mechanisms and clinical relevance in atrial fibrillation. *J. Am. Coll. Cardiol.* **51**, 802–809 (2008).
25. Van Wagoner, D. R. Basic mechanisms of atrial fibrillation. *Cleve Clin. J. Med.* **70**, S2–S5 (2003).

26. Shapiro-Shelef, M. et al. Blimp-1 is required for the formation of immunoglobulin secreting plasma cells and pre-plasma memory B cells. *Immunity* **19**, 607–620 (2003).
27. Setz, C. S. et al. PI3K-mediated blimp-1 activation controls B cell selection and homeostasis. *Cell Rep.* **24**, 391–405 (2018).
28. Hu, B. et al. Association of β1-adrenergic, M2-muscarinic receptor autoantibody with occurrence and development of nonvalvular atrial fibrillation. *Pacing Clin. Electrophysiol.* **39**, 1379–1387 (2016).
29. Shang, L. et al. Elevated β1-adrenergic receptor autoantibody levels increase atrial fibrillation susceptibility by promoting atrial fibrosis. *Front. Physiol.* **11**, 76 (2020).
30. Christ, T. et al. Autoantibodies against the beta1 adrenoceptor from patients with dilated cardiomyopathy prolong action potential duration and enhance contractility in isolated cardiomyocytes. *J. Mol. Cell. Cardiol.* **33**, 1515–1525 (2001).
31. Manders, E. M. M., Verbeek, F. J. & Aten, J. A. Measurement of co-localization of objects in dual-colour confocal images. *J. Microsc.* **169**, 375–382 (1993).
32. Huke, S. & Bers, D. M. Ryanodine receptor phosphorylation at Serine 2030, 2808 and 2814 in rat cardiomyocytes. *Biochem. Biophys. Res. Commun.* **376**, 80–85 (2008).
33. Salles, G. et al. Rituximab in B-cell hematologic malignancies: a review of 20 years of clinical experience. *Adv. Ther.* **34**, 2232–2273 (2017).
34. van Vollenhoven, R. F. et al. Long-term safety of rituximab in rheumatoid arthritis: 9.5-year follow-up of the global clinical trial programme with a focus on adverse events of interest in RA patients. *Ann. Rheum. Dis.* **72**, 1496–1502 (2013).
35. Wijffels, M. C., Kirchhof, C. J., Dorland, R. & Allessie, M. A. Atrial fibrillation begets atrial fibrillation. A study in awake chronically instrumented goats. *Circulation* **92**, 1954–1968 (1995).
36. Fukuda, Y. et al. Autoimmunity against the second extracellular loop of β_1-adrenergic receptors induces early afterdepolarization and decreases in K-channel density in rabbits. *J. Am. Coll. Cardiol.* **43**, 1090–1100 (2004).
37. Heijman, J., Voigt, N., Nattel, S. & Dobrev, D. Cellular and molecular electrophysiology of atrial fibrillation initiation, maintenance, and progression. *Circ. Res.* **114**, 1483–1499 (2014).
38. Franz, M. R., Jamal, S. M. & Narayan, S. M. The role of action potential alternans in the initiation of atrial fibrillation in humans: a review and future directions. *Europace* **14**, v58–v64 (2012).
39. William, J., Euler, C., Christensen, S. & Shlomchik, M. J. Evolution of autoantibody responses via somatic hypermutation outside of germinal centers. *Science* **297**, 2066–2070 (2002).
40. Jenks, S. A. et al. Distinct effector B cells induced by unregulated toll-like receptor 7 contribute to pathogenic responses in systemic lupus erythematosus. *Immunity* **49**, 725–739.e6 (2018).
41. Soni, C. et al. Plasmacytoid dendritic cells and type I interferon promote extrafollicular B cell responses to extracellular self-DNA. *Immunity* **52**, 1022–1038.e7 (2020).
42. Baba, A. et al. Autoantibodies: new upstream targets of paroxysmal atrial fibrillation in patients with congestive heart failure. *J. Cardiol.* **40**, 217–223 (2002).
43. Maguy, A., Mahendran, Y., Tardif, J. C., Busseuil, D. & Li, J. Autoimmune atrial fibrillation. *Circulation* **148**, 487–498 (2023).
44. Hindricks, G. et al. 2020 ESC Guidelines for the diagnosis and management of atrial fibrillation developed in collaboration with the European Association for Cardio-Thoracic Surgery (EACTS): The Task Force for the diagnosis and management of atrial fibrillation of the European Society of Cardiology (ESC) Developed with the special contribution of the European Heart Rhythm Association (EHRA) of the ESC. *Eur. Heart J.* **42**, 373–498 (2021).
45. Golf, S. & Hansson, V. Effects of beta blocking agents on the density of beta adrenoceptors and adenylate cyclase response in human myocardium: intrinsic sympathomimetic activity favours receptor upregulation. *Cardiovasc. Res.* **20**, 637–644 (1986).
46. Lee, D. S. W., Rojas, O. L. & Gommerman, J. L. B cell depletion therapies in autoimmune disease: advances and mechanistic insights. *Nat. Rev. Drug Discov.* **20**, 179–199 (2021).
47. Tschöpe, C. et al. Targeting $CD20^+$ B-lymphocytes in inflammatory dilated cardiomyopathy with rituximab improves clinical course: a case series. *Eur. Heart J. Case Rep.* **3**, ytz131 (2019).
48. Zhao, T. X. et al. Rituximab in patients with acute ST-elevation myocardial infarction: an experimental medicine safety study. *Cardiovasc. Res.* **118**, 872–882 (2022).
49. Crickx, E., Weill, J.-C., Reynaud, C.-A. & Mahévas, M. Anti-CD20-mediated B-cell depletion in autoimmune diseases: successes, failures and future perspectives. *Kidney Int.* **97**, 885–893 (2020).
50. Wallukat, G. et al. Aptamer BC007 for neutralization of pathogenic autoantibodies directed against G-protein coupled receptors: a vision of future treatment of patients with cardiomyopathies and positivity for those autoantibodies. *Atherosclerosis* **244**, 44–47 (2016).
51. Zheng, Z. et al. Perioperative rosuvastatin in cardiac surgery. *N. Engl. J. Med.* **374**, 1744–1753 (2016).
52. Bapat, A. et al. Genetic inhibition of serum glucocorticoid kinase 1 prevents obesity-related atrial fibrillation. *JCI Insight* **7**, e160885 (2022).
53. Winer, D. A. et al. B cells promote insulin resistance through modulation of T cells and production of pathogenic IgG antibodies. *Nat. Med.* **17**, 610–617 (2011).
54. Tan, J. J. et al. Human iPS-derived pre-epicardial cells direct cardiomyocyte aggregation expansion and organization in vitro. *Nat. Commun.* **12**, 4997 (2021).
55. Pabel, S. et al. Dantrolene reduces CaMKIIδC-mediated atrial arrhythmias. *Europace* **22**, 1111–1118 (2020).
56. Ackers-Johnson, M. et al. A Simplified, Langendorff-free method for concomitant isolation of viable cardiac myocytes and nonmyocytes from the adult mouse heart. *Circ. Res.* **119**, 909–920 (2016).
57. Dress, R. J., Wong, A. Y. & Ginhoux, F. Homeostatic control of dendritic cell numbers and differentiation. *Immunol. Cell Biol.* **96**, 463–476 (2018).
58. Lorenzo, C. et al. ALDH4A1 is an atherosclerosis auto-antigen targeted by protective antibodies. *Nature* **589**, 287–292 (2021).
59. Pracht, K. et al. A new staining protocol for detection of murine antibody-secreting plasma cell subsets by flow cytometry. *Eur. J. Immunol.* **47**, 1389–1392 (2017).
60. Stuart, T. et al. Comprehensive integration of single-cell data. *Cell* **177**, 1888–1902.e21 (2019).
61. Butler, A., Hoffman, P., Smibert, P., Papalexi, E. & Satija, R. Integrating single-cell transcriptomic data across different conditions, technologies, and species. *Nat. Biotechnol.* **36**, 411–420 (2018).
62. Hafemeister, C. & Satija, R. Normalization and variance stabilization of single-cell RNA-seq data using regularized negative binomial regression. *Genome Biol.* **20**, 296 (2019).
63. Lun, A. T. L. & Marioni, J. C. Overcoming confounding plate effects in differential expression analyses of single-cell RNA-seq data. *Biostatistics* **18**, 451–464 (2017).
64. Chen, Y., Lun, A. T. & Smyth, G. K. From reads to genes to pathways: differential expression analysis of RNA-Seq experiments using Rsubread and the edgeR quasi-likelihood pipeline. *F1000Res.* **5**, 1438 (2016).
65. McCarthy, D. J., Chen, Y. & Smyth, G. K. Differential expression analysis of multifactor RNA-seq experiments with respect to biological variation. *Nucleic Acids Res.* **40**, 4288–4297 (2012).
66. Robinson, M. D., McCarthy, D. J. & Smyth, G. K. edgeR: a Bioconductor package for differential expression analysis of digital gene expression data. *Bioinformatics* **26**, 139–140 (2010).

67. Subramanian, A. et al. Gene set enrichment analysis: a knowledge-based approach for interpreting genome-wide expression profiles. *Proc. Natl Acad. Sci. USA* **102**, 15545–15550 (2005).
68. Mootha, V. K. et al. PGC-1alpha-responsive genes involved in oxidative phosphorylation are coordinately downregulated in human diabetes. *Nat. Genet.* **34**, 267–273 (2003).
69. Liberzon, A. et al. Molecular signatures database (MSigDB) 3.0. *Bioinformatics* **27**, 1739–1740 (2011).

Acknowledgements

We acknowledge Servier Medical Art (smart.servier.com) and BioRender (IH23GLWC6I) for cartoon components. We acknowledge K. Joyce for editing the manuscript. This work was supported by a grant from the Leducq Foundation, National Institutes of Health (grants HL155097 (M.H.), HL149647 (M.H.), HL142494 (F.K.S., K.N. and M.N.), HL176359 (M.N.), CA225655 (K.N.), HL007604 (A.B.), HL158040 (F.E.P.), HL135752 (F.K.S.), HL157635 (P.T.E.), HL139731 (P.T.E.), HL092577 (P.T.E.)); Japan Heart Foundation/Bayer Yakuhin Research Grant Abroad (M.Y.); Deutsche Forschungsgemeinschaft (DFG) 453989101 SFB 1525 Mercator fellow (M.N.); DFG #491497342 (N.K.); DFG 530157297 (S.P.); DFG (M.J.S), Else-Kröner-Fresenius Stiftung 2019/A84 (S.P.); Max Kade Foundation/Austrian Academy of Sciences (T.D.); British Heart Foundation RG/18/3/34214 and CH/12/3/29609 (A.L., C.A. and B.C.); NIHR Oxford Biomedical Research Centre (A.L., C.A. and B.C.); American Heart Association 18SFRN34110082 (P.T.E) and European Union MAESTRIA 965286 (C.A. and P.T.E).

Author contributions

M.Y., K.K.Y.T. and S.P. conceived the study; designed, performed and analyzed experiments; interpreted data and made the figures. I.L., A.B., L.X., F.E.P., K.M., A.P., N.M., H.S., T.D., N.K., M.J.S and Y.I. designed, performed and analyzed experiments. A.L., K.C., C.A. and B.C. provided human data. G.R., F.K.S., P.T.E. and K.N. discussed results and strategy. S.P., M.H. and M.N. conceived and directed the study. M.Y., S.P., M.H. and M.N. wrote the manuscript with input from all authors.

Competing interests

P.T.E. receives funds or material research support from Bayer AG, IBM Research, Bristol Myers Squibb, Pfizer, MyoKardia and Novartis. M.N. has received funds or material research support from Alnylam, Biotronik, CSL Behring, GlycoMimetics, GSK, Medtronic, Novartis and Pfizer, as well as consulting fees from Biogen, Gimv, IFM Therapeutics, Molecular Imaging, Sigilon, Verseau Therapeutics and Bitterroot. S.P. is employed by the Novartis Institute of Biomedical Research. The other authors declare no competing interests.

Additional information

Extended data is available for this paper at https://doi.org/10.1038/s44161-025-00724-z.

Supplementary information The online version contains supplementary material available at https://doi.org/10.1038/s44161-025-00724-z.

Correspondence and requests for materials should be addressed to Steffen Pabel, Maarten Hulsmans or Matthias Nahrendorf.

Peer review information *Nature Cardiovascular Research* thanks the anonymous reviewer(s) for their contribution to the peer review of this work.

Reprints and permissions information is available at www.nature.com/reprints.

Publisher's note Springer Nature remains neutral with regard to jurisdictional claims in published maps and institutional affiliations.

[1]Center for Systems Biology, Massachusetts General Hospital and Harvard Medical School, Boston, MA, USA. [2]Department of Radiology, Massachusetts General Hospital and Harvard Medical School, Boston, MA, USA. [3]Cardiovascular Research Center, Massachusetts General Hospital and Harvard Medical School, Boston, MA, USA. [4]Radcliffe Department of Medicine, NIHR Biomedical Research Centre, University of Oxford, Oxford, UK. [5]British Heart Foundation Centre of Research Excellence, University of Oxford, Oxford, UK. [6]Cardiovascular Disease Initiative, The Broad Institute of MIT and Harvard University, Cambridge, MA, USA. [7]Department of Internal Medicine I/Comprehensive Heart Failure Center, University Hospital Wuerzburg, Wuerzburg, Germany. [8]Cardiovascular Research Institute, Icahn School of Medicine at Mount Sinai, New York, NY, USA. [9]Department of Medicine, Icahn School of Medicine at Mount Sinai, New York, NY, USA. [10]Blavatnik Institute, Department of Genetics, Harvard Medical School, Boston, MA, USA. [11]Department of Internal Medicine II, University Hospital Regensburg, Regensburg, Germany. [12]MGB Center for Inflammation Imaging, Massachusetts General Hospital and Harvard Medical School, Boston, MA, USA. [13]These authors jointly supervised this work: Steffen Pabel, Maarten Hulsmans, Matthias Nahrendorf. ✉e-mail: steffen.pabel@gmail.com; mhulsmans@mgh.harvard.edu; mnahrendorf@mgh.harvard.edu

https://doi.org/10.1038/s44161-025-00724-z

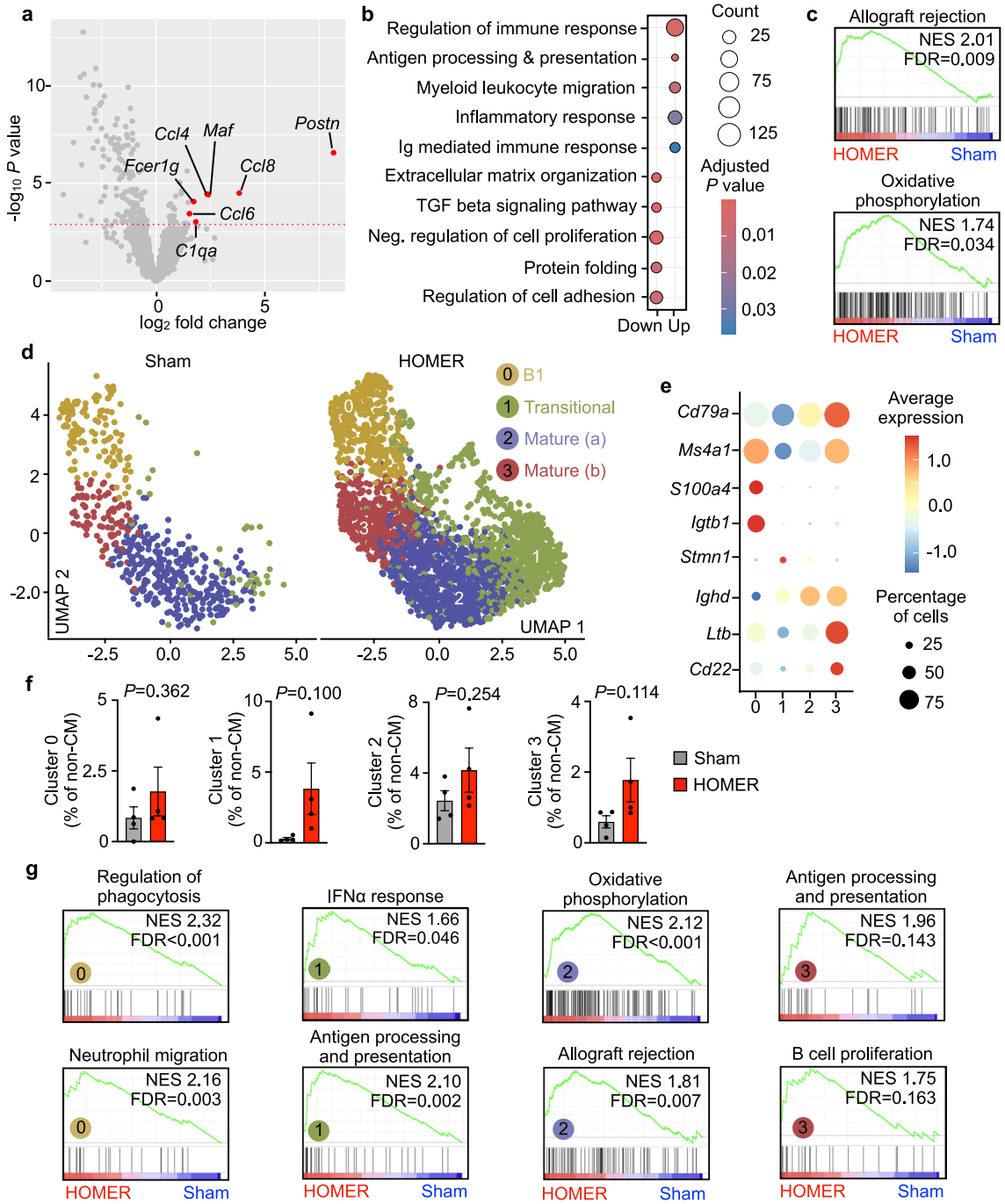

Extended Data Fig. 1 | Atrial B cell subset phenotype change in HOMER mice. **a**, Volcano plot of significantly upregulated genes in atrial B cells of HOMER mice. Marked genes are associated with inflammatory response and antigen presentation and have an FDR < 0.05. **b**, Significant gene ontology biological process (GOBP) gene sets, highlighting major up- or down-regulated gene sets in B cells in HOMER mice ($n = 4$) compared with control mice ($n = 4$). Dot color indicates statistical significance and dot size the number of enriched genes. **c**, Gene set enrichment analysis (GSEA) plots highlighting upregulated inflammatory pathways in B cells of HOMER mice. **d**, Dimensionality reduction analysis by UMAP shows 4 B cell populations. **e**, Dot plot annotating B cell clusters by signature gene expression. Color denotes *z*-score of average gene expression (red, high; blue, low); circle size indicates percentage of cells expressing the gene. **f**, Relative cell population frequencies of B cell subclusters. $n = 4$ per group (biological replicates). Data are the mean±s.e.m. with individual values for data distribution. Two-tailed Student's *t*-test. **g**, GSEA plots highlighting upregulated pathways in B cell subclusters of HOMER mice.

https://doi.org/10.1038/s44161-025-00724-z

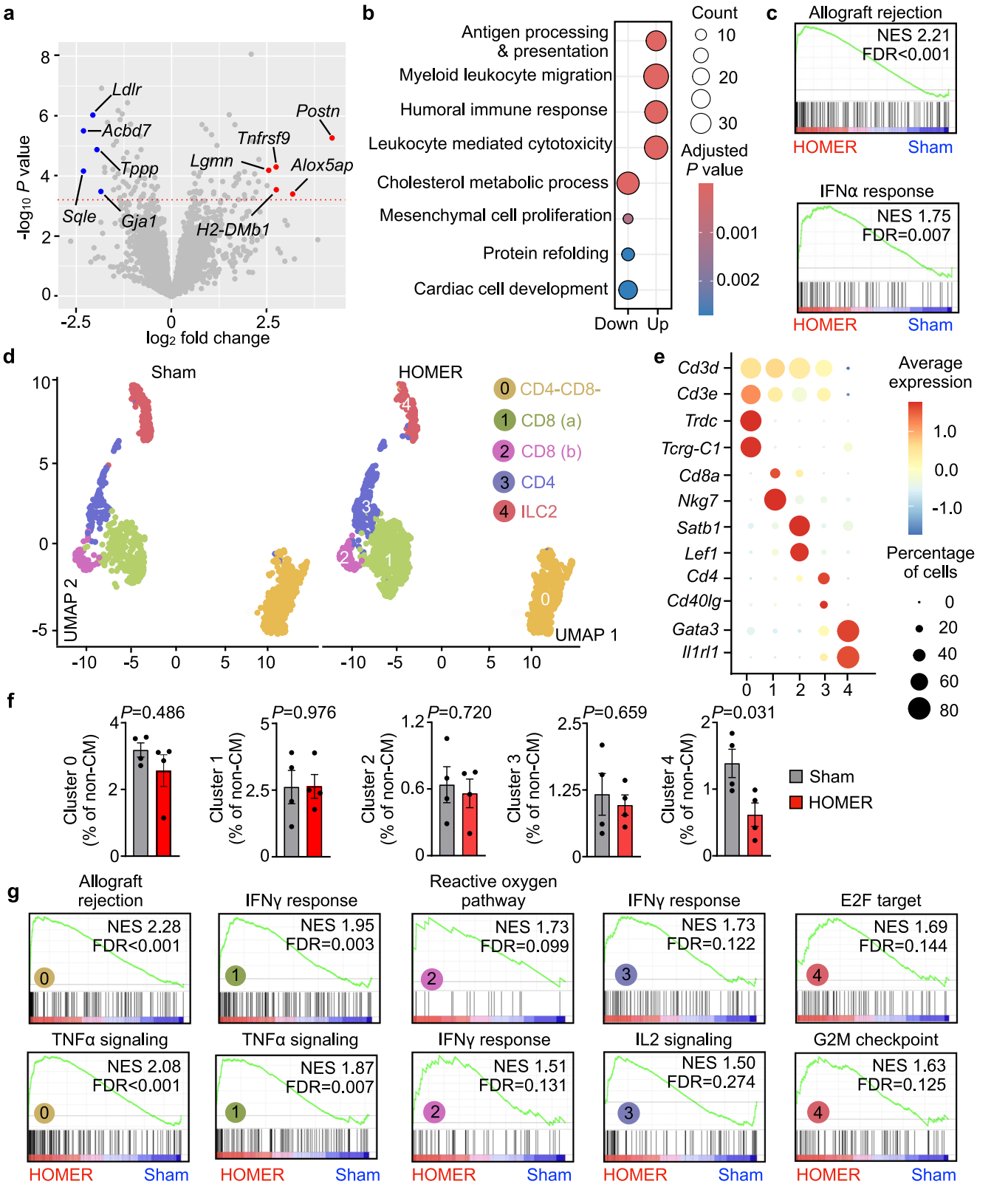

Extended Data Fig. 2 | Atrial T cell subset phenotype change in HOMER mice. **a**, Volcano plot of significantly regulated genes in atrial T cells of HOMER mice. Marked genes are most regulated by fold-change and have an FDR < 0.05. **b**, Significant GOBP gene sets, highlighting major up- or down-regulated gene sets in atrial T cells of HOMER mice ($n = 4$) compared with control mice ($n = 4$). Dot color indicates statistical significance and dot size the number of enriched genes. **c**, GSEA plots highlighting upregulated inflammatory pathways in T cells of HOMER mice. **d**, Dimensionality reduction analysis by UMAP shows 5 T cell populations. **e**, Dot plot annotating T cell clusters by signature gene expression. Color denotes *z*-score of average gene expression (red, high; blue, low); circle size indicates percentage of cells expressing the gene. **f**, Relative cell population frequencies of T cell subcluster. $n = 4$ per group (biological replicates). Data are the mean±s.e.m. with individual values for data distribution. Two-tailed Student's *t*-test. **g**, GSEA plots highlighting upregulated pathways in T cell subclusters of HOMER mice.

https://doi.org/10.1038/s44161-025-00724-z

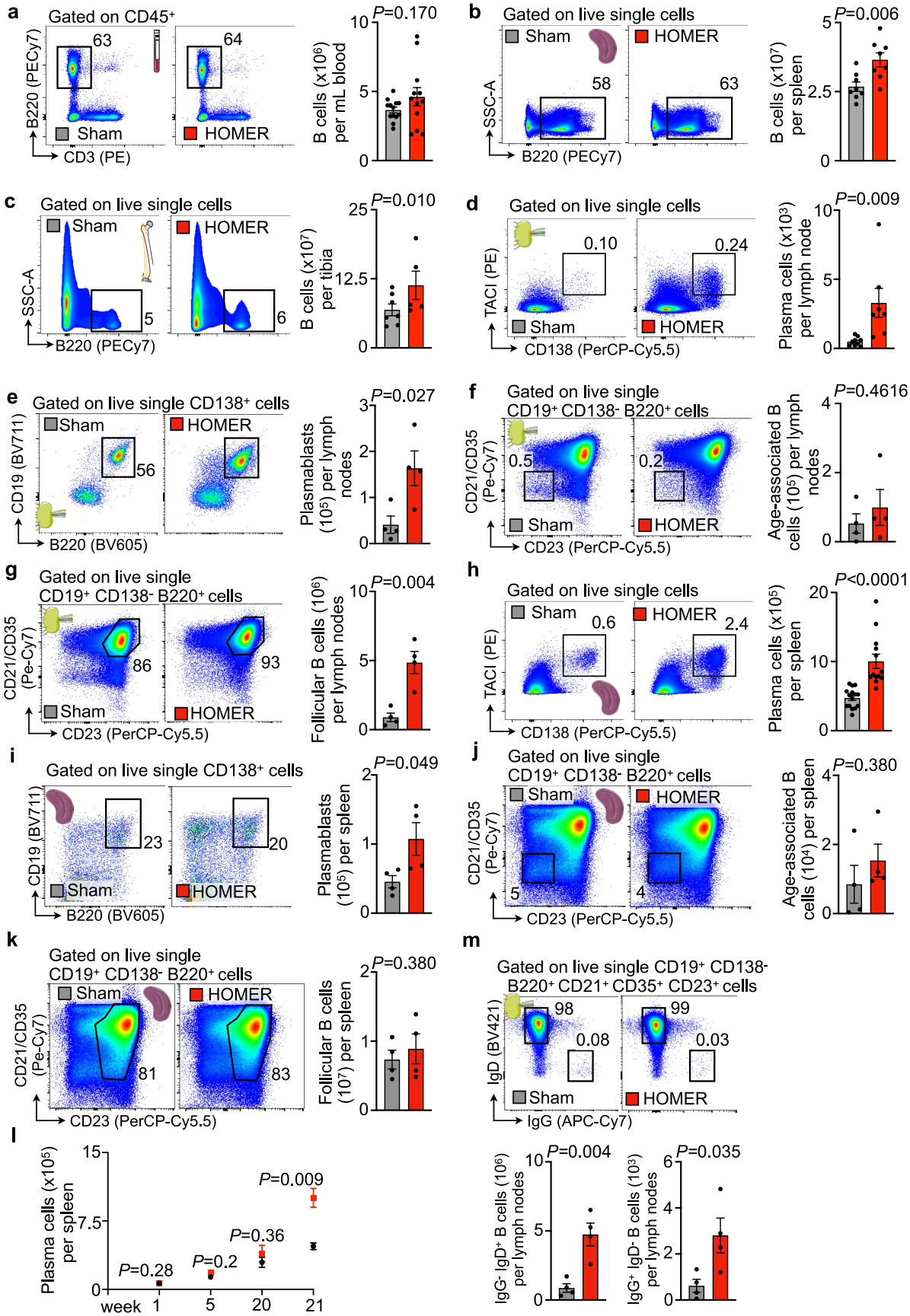

Extended Data Fig. 3 | See next page for caption.

https://doi.org/10.1038/s44161-025-00724-z

Extended Data Fig. 3 | B cell response in HOMER mice. a-c, A flow cytometric quantification of B cells in blood (**a**, *n* = 13 and 12 per group), spleen (**b**, *n* = 8 per group) and bone marrow (**c**, *n* = 7 and 5 per group) from sham and HOMER mice. Two-tailed Student's *t*-test. **d-g**, A flow cytometric quantification of plasma cells (**d**), plasma blasts (**e**), age-associated B cells (**f**) and follicular B cells (**g**) in mediastinal lymph nodes from sham and HOMER mice. *n* = 4 per group, two-tailed Student's *t*-test. **h-k**, Flow cytometric quantification of plasma cells (**h**, *n* = 15 and 13 per group), plasmablasts (**i**, *n* = 4 per group), age-associated B cells (**j**, *n* = 4 per group) and follicular B cells (**k**, *n* = 4 per group) in the spleen from sham and HOMER mice. Two-tailed Student's *t*-test. **l**, Time course of plasma cells at 1 (1 week after sham or MR surgery, *n* = 5 per group), 5 (1 week after HFD initiation, *n* = 5 and 6 per group), 20 (*n* = 7 and 6 per group) and 21 weeks (before and 1 week after angiotensin-2 infusion, *n* = 15 and 13 per group) in spleen from sham and HOMER mice quantified by flow cytometry. Two-tailed Student's *t*-test. **m**, A flow cytometric quantification of IgG^- IgD^+ and IgG^+ IgD^- B cell subsets in mediastinal lymph nodes from sham and HOMER mice. *n* = 4 per group, two-tailed Student's *t*-test. Data are the mean±s.e.m. with individual values for data distribution.

https://doi.org/10.1038/s44161-025-00724-z

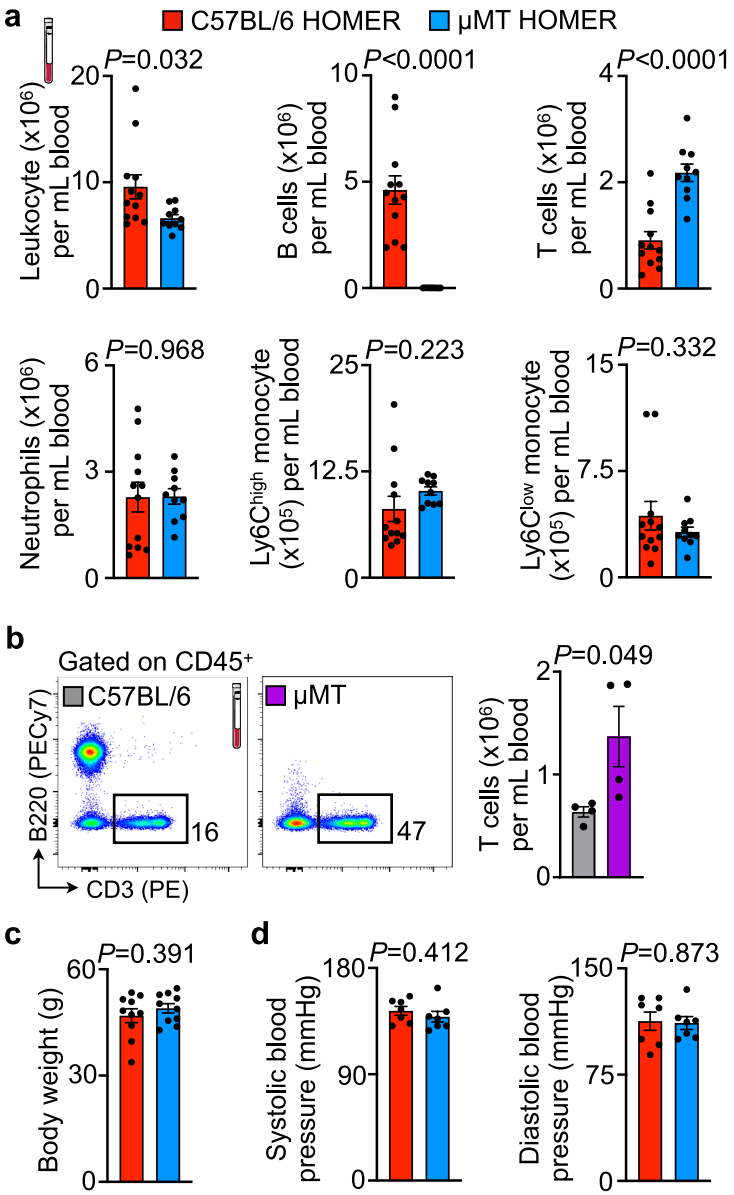

Extended Data Fig. 4 | C57BL/6 and µMT HOMER mice characteristics. **a**, A flow cytometric quantification of total leukocytes, B cells, T cells, neutrophils and monocytes in blood from C57BL/6 and µMT HOMER mice. $n = 12$ and 10 per group, two-tailed Student's t-test. **b**, A flow cytometric quantification of T cells in the blood from naive C57BL/6 and naive µMT mice. $n = 4$ per group, two-tailed Student's t-test. **c**, Body weight of C57BL/6 and µMT HOMER mice. $n = 10$ per group, two-tailed Student's t-test. **d**, Systolic (left) and diastolic (right) blood pressure of C57BL/6 and µMT HOMER mice. $n = 10$ per group, two-tailed Student's t-test. Data are the mean±s.e.m. with individual values for data distribution.

https://doi.org/10.1038/s44161-025-00724-z

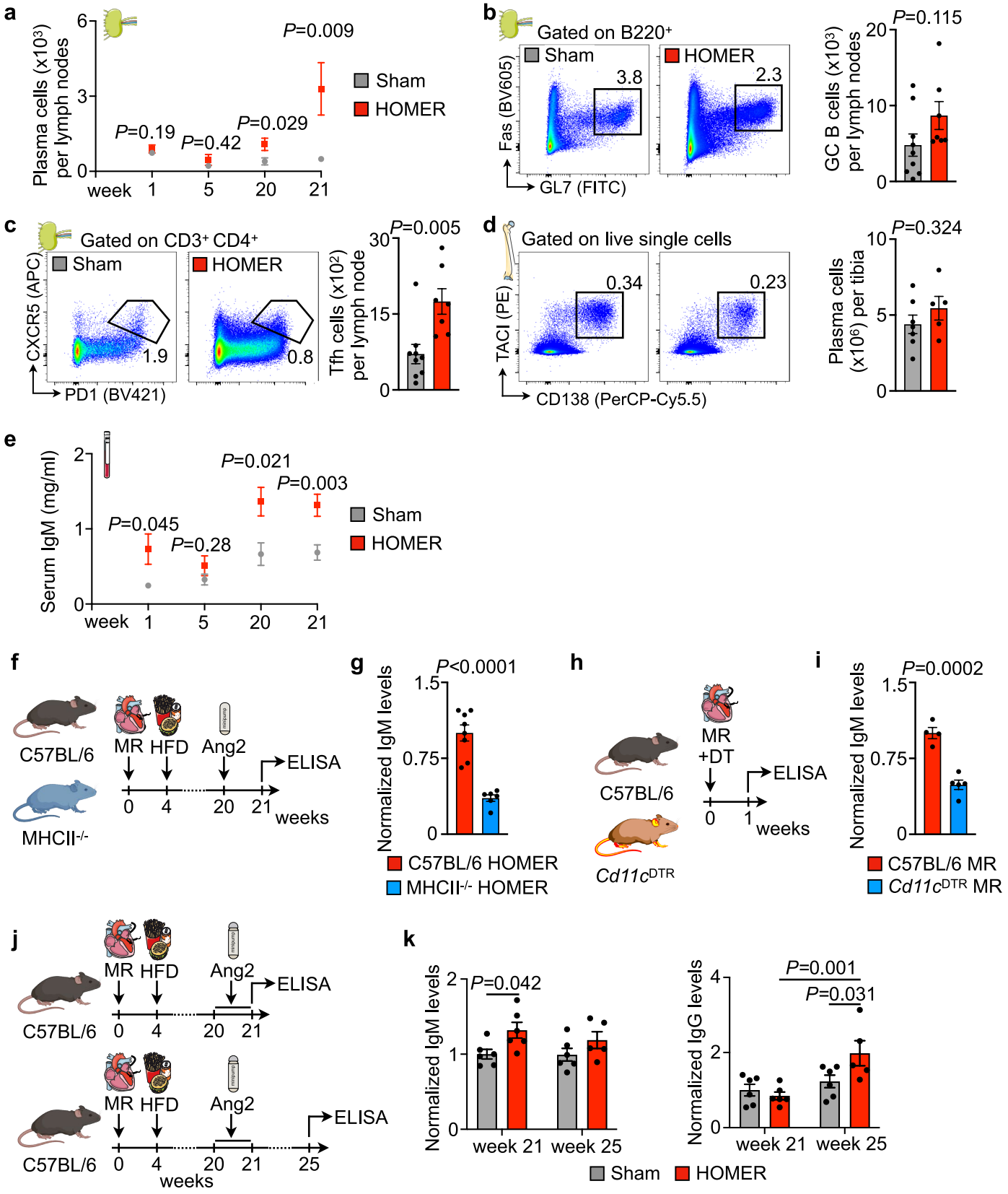

Extended Data Fig. 5 | See next page for caption.

https://doi.org/10.1038/s44161-025-00724-z

Extended Data Fig. 5 | Plasma cells and serum IgM in HOMER mice, antigen presentation and immunoglobuline kinetics. a, Time course of plasma cells at 1 (1 week after sham or MR surgery, $n = 5$ per group), 5 (1 week after HFD initiation, $n = 4$ and 6 per group), 20 ($n = 7$ and 6 per group) and 21 weeks (before and 1 week after angiotensin-2 infusion, $n = 9$ and 7 per group) in mediastinal lymph nodes from sham and HOMER mice quantified by flow cytometry. Two-tailed Student's *t*-test, *P* values are compared with sham at each time point. **b**, A flow cytometric quantification of germinal center (GC) B cells in mediastinal lymph nodes from sham and HOMER mice. $n = 9$ and 7 per group, two-tailed Student's *t*-test. **c**, A flow cytometric quantification of T follicular helper (Tfh) cells in mediastinal lymph nodes from sham and HOMER mice. $n = 9$ and 7 per group, two-tailed Student's *t*-test. **d**, A flow cytometric quantification of plasma cells in tibia from sham and HOMER mice $n = 7$ to 5 per group, two-tailed Student's *t*-test. **e**, Time course of serum IgM in sham and HOMER mice at 1 ($n = 5$ per group), 5 ($n = 5$ and 6 per group), 20 ($n = 5$ per group) and 21 weeks ($n = 9$ per group) quantified with ELISA. Two-tailed Student's *t*-test, *P* values are compared with sham at each time point. **f**, Experimental outline: C57BL/6 and MHCII$^{-/-}$ mice are exposed to the HOMER protocol followed by quantification of IgM levels by ELISA. **g**, Serum IgM levels in C57BL/6 and MHCII$^{-/-}$ HOMER mice. $n = 6$ and 8 per group, two-tailed Student's *t*-test. **h**, Experimental outline: C57BL/6 and *Cd11c*^{DTR} mice are injected with diphtheria toxin and exposed to MR surgery for 1 week followed by quantification of IgM levels by ELISA. **i**, Serum IgM levels in C57BL/6 MR and *Cd11c*^{DTR} MR mice. $n = 4$ and 5 per group, two-tailed Student's *t*-test. **j**, Experimental outline: IgM and IgG ELISA of HOMER serum was performed at week 21 and 25. **k**, Blood IgM and IgG levels in sham and HOMER mice at the endpoint of the HOMER protocol (week 21, $n = 6$ per group) or 4 weeks later (week 25, $n = 6$ and 5 per group) by ELISA. Two-tailed Student's *t*-test. Data are the mean±s.e.m. with individual values for data distribution.

https://doi.org/10.1038/s44161-025-00724-z

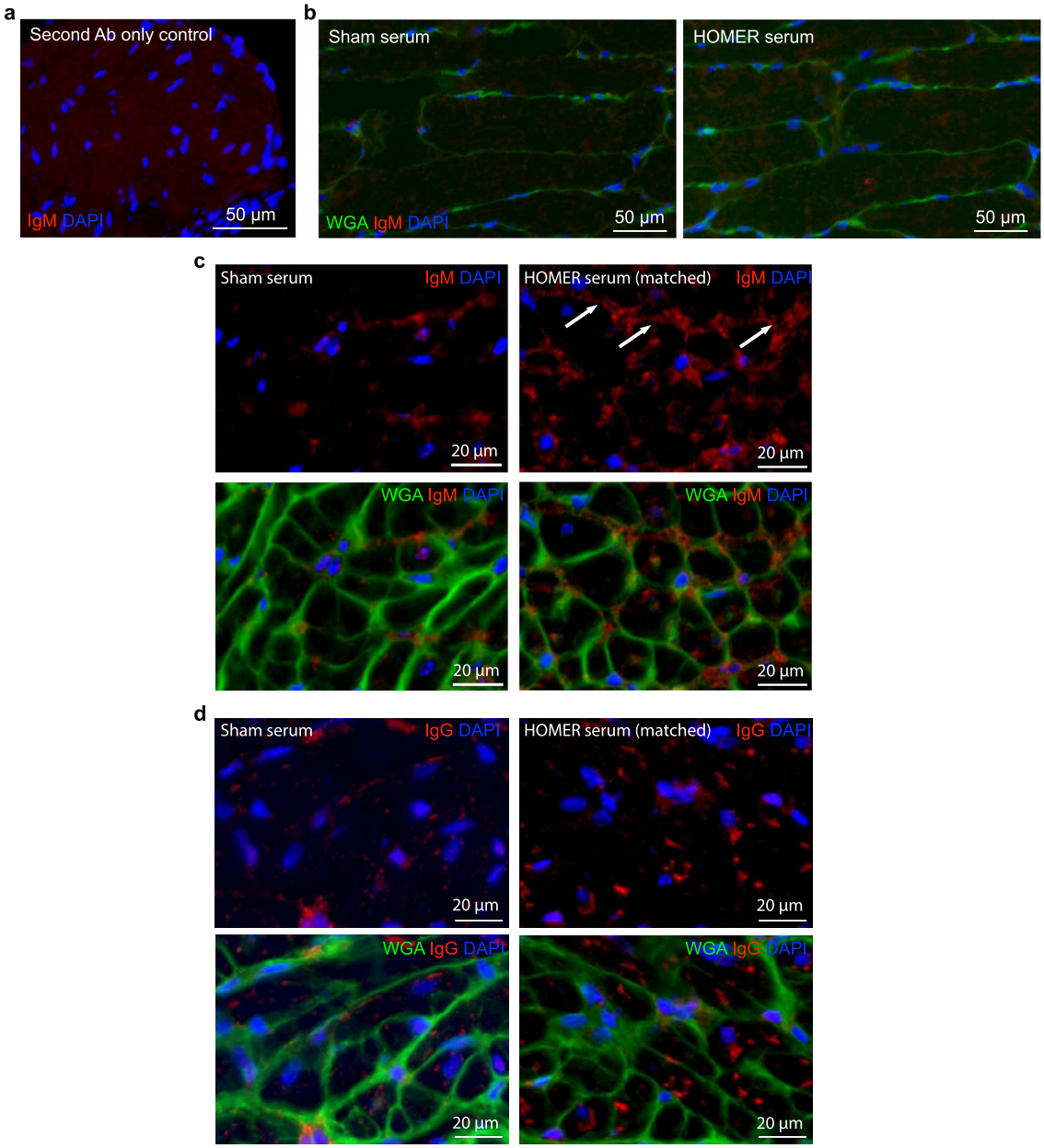

Extended Data Fig. 6 | IgM deposition in the atria. a, A representative staining of IgM in µMT HOMER left atria with secondary antibody only ($n = 2$). **b**, A representative staining of IgM in µMT HOMER skeletal muscle with C57BL/6 sham or HOMER serum. Representative stainings are shown for sera form $n = 3$ sham and $n = 3$ HOMER mice. **c**, A staining of IgM in µMT HOMER left atria with concentration-matched C57BL/6 sham and HOMER serum. Co-staining was done with WGA for cell membranes. Arrows indicate IgM deposits on cell membranes. Representative stainings are shown for sera from $n = 5$ sham and $n = 8$ HOMER mice. **d**, A staining of IgG in µMT HOMER left atria with concentration-matched C57BL/6 sham and HOMER serum obtained right after completion of the HOMER procedures, a time point where IgG levels are still lower than IgM levels. Representative stainings are shown for sera from $n = 3$ sham and $n = 3$ HOMER mice.

https://doi.org/10.1038/s44161-025-00724-z

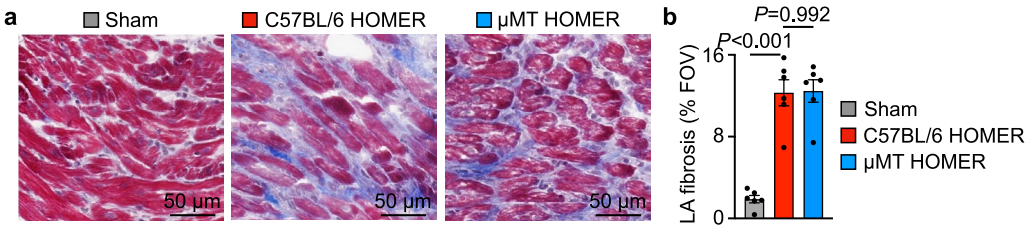

Extended Data Fig. 7 | Effects of B cells on atrial fibrosis in HOMER mice. **a**, A representative Masson's trichrome staining for fibrosis in left atria from sham, C57BL/6 HOMER and μMT HOMER mice. **b**, Quantification of fibrotic area in left atria from sham, C57BL/6 HOMER and μMT HOMER mice. $n = 6$ per group. Data are the mean±s.e.m. with individual values for data distribution. One-way ANOVA followed by Tukey's multiple comparisons test. FOV, field of view.

https://doi.org/10.1038/s44161-025-00724-z

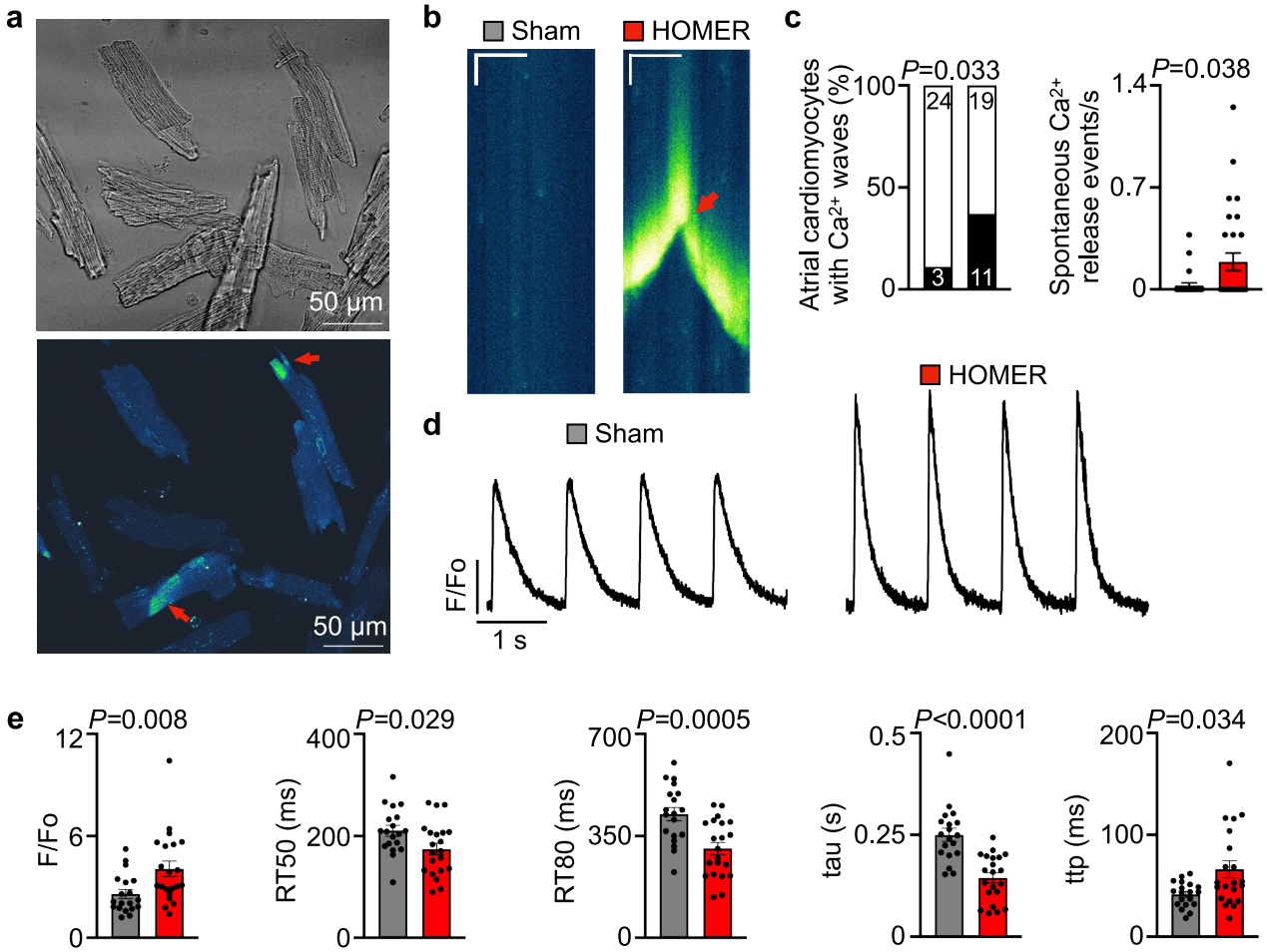

Extended Data Fig. 8 | Calcium handling in HOMER atrial cardiomyocytes. **a**, Isolated cardiomyocytes loaded with the calcium dye Fluo-4. Arrows indicate spontaneous diastolic calcium wave. Numbers of cardiomyocytes studied is indicated in **c**. **b**, Original line scans from atrial cardiomyocytes isolated from sham or HOMER mice. Arrow indicates a spontaneous diastolic calcium wave. Scale bar: x = 20 µm, y = 100 ms. **c**, Percentage of atrial cardiomyocytes from sham and HOMER mice with spontaneous calcium waves and frequency of calcium release events. *n* = 27 and 30 per group, two-sided Fisher's exact test or two-tailed Mann-Whitney test. **d**, Representative tracings of stimulated systolic calcium transients in atrial cardiomyocytes from sham and HOMER mice. **e**, Calcium transient amplitude (F/F_0), relaxation time 50% (RT50) and 80% (RT80), exponential decay time constant (tau) and time to peak (ttp) of systolic calcium transients in atrial cardiomyocytes from sham and HOMER mice. *n* = 27 and 30 per group, two-tailed Student's *t*-test. Data are the mean±s.e.m. with individual values for data distribution.

https://doi.org/10.1038/s44161-025-00724-z

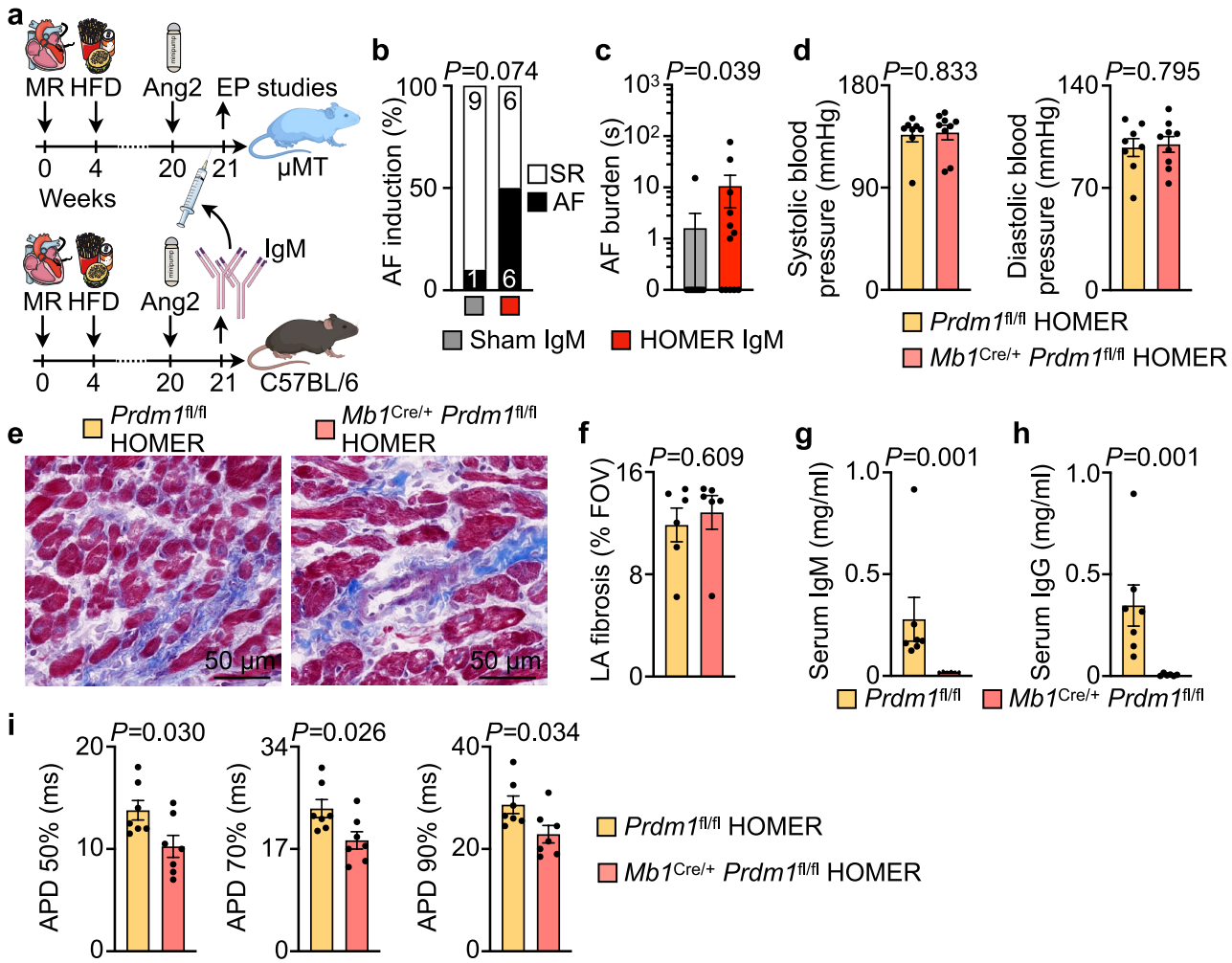

Extended Data Fig. 9 | Antibody contributions to inducible AF. a, Experimental outline: IgM extracted from C57BL/6 sham or HOMER mice serum was injected into μMT HOMER mice 2 days before EP study. **b**, EP study of AF inducibility in sham IgM- or HOMER IgM-injected mice. $n = 10$ and 12 per group, two-sided Fisher's exact test. **c**, EP study of AF burden in sham IgM- or HOMER IgM-injected mice. $n = 10$ and 12 per group, two-tailed Mann-Whitney test. **d**, Systolic (left) and diastolic (right) blood pressure of *Prdm1*$^{fl/fl}$ HOMER and *Mb1*$^{Cre/+}$ *Prdm1*$^{fl/fl}$ HOMER mice. $n = 8$ and 9 per group, two-tailed Student's *t*-test. **e**, A representative Masson's trichrome staining for fibrosis in left atria from *Prdm1*$^{fl/fl}$ HOMER and *Mb1*$^{Cre/+}$ *Prdm1*$^{fl/fl}$ HOMER mice. **f**, Quantification of fibrotic area in left atria from *Prdm1*$^{fl/fl}$ HOMER and *Mb1*$^{Cre/+}$ *Prdm1*$^{fl/fl}$ HOMER mice. $n = 6$ per group, two-tailed Student's *t*-test. **g**,**h**, Baseline serum IgM (**g**) and IgG (**h**) levels in *Prdm1*$^{fl/fl}$ and *Mb1*$^{Cre/+}$ *Prdm1*$^{fl/fl}$ mice quantified with ELISA. $n = 6$ and 8 per group, two-tailed Mann-Whitney test. **i**, Quantification of action potential duration 50%, 75% and 90% in left atria from *Prdm1*$^{fl/fl}$ HOMER and *Mb1*$^{Cre/+}$ *Prdm1*$^{fl/fl}$ HOMER mice. $n = 7$ per group, two-tailed Student's *t*-test. Data are the mean±s.e.m. with individual values for data distribution.

https://doi.org/10.1038/s44161-025-00724-z

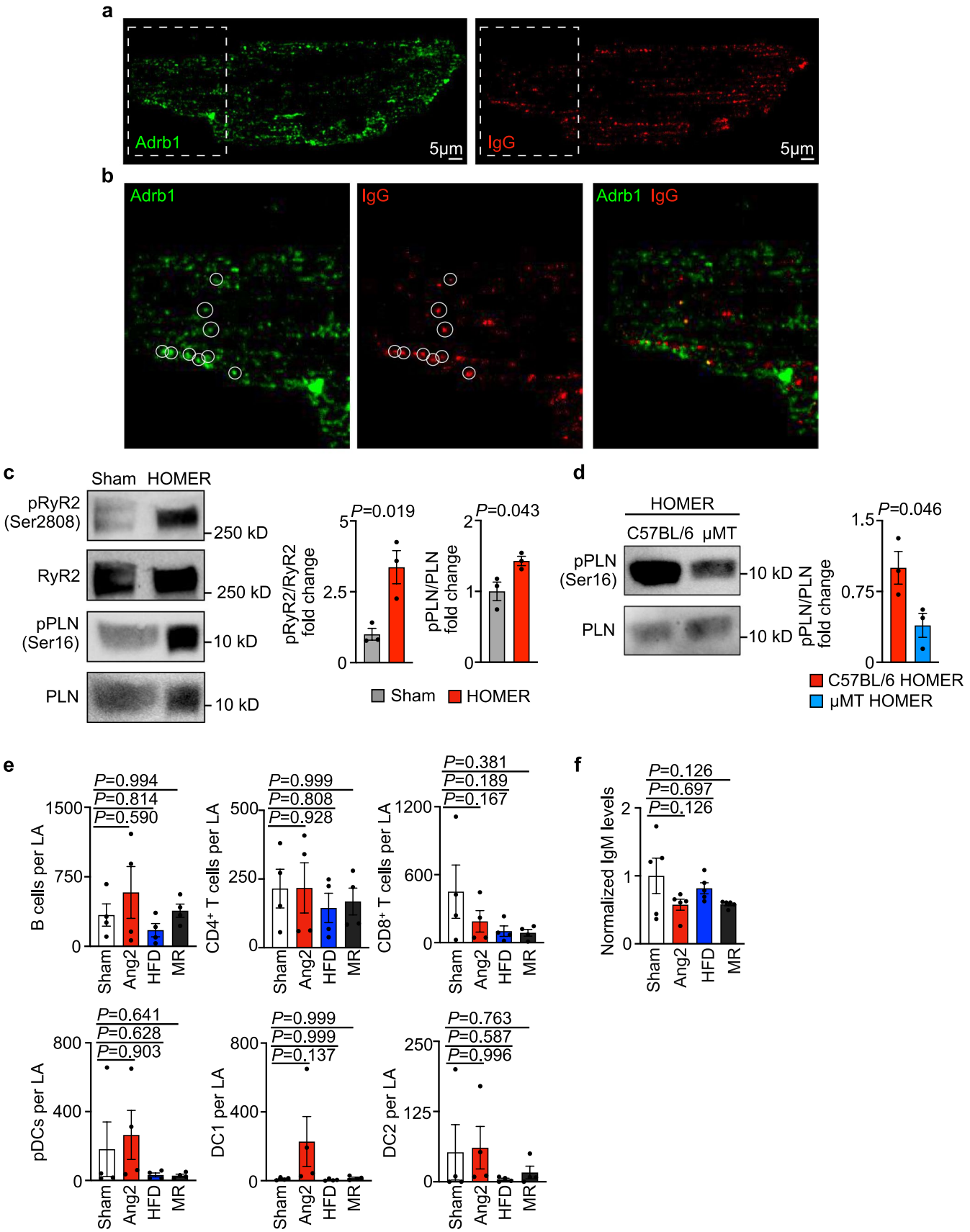

Extended Data Fig. 10 | See next page for caption.

https://doi.org/10.1038/s44161-025-00724-z

Extended Data Fig. 10 | HOMER IgG binding, calcium handling and effects of single HOMER components. a, A representative double staining for Adrb1 (left, green) and purified HOMER IgG (right, red) acquired 4 weeks after completion of the HOMER protocol in cardiomyocytes isolated from adult C57BL/6 mice. Representative stainings are shown for purified IgG from 2 HOMER mice. **b**, Higher magnification of the boxed area indicated in **a** for Adrb1 (left) and IgG (middle) staining. Circles indicate signal colocalization of Adrb1 and IgM. Overlay (right) of Adrb1 and IgM signal in a cardiomyocyte isolated from an adult C57BL/6 mouse. **c**, Western blot showing p2808 RyR2, total RyR2 protein expression, p16 phospholamban (PLN) and total PLN expression in left atria tissues from sham and HOMER mice. $n = 3$ per group, two-tailed Student's *t*-test. **d**, Western blot showing p16 PLN and total PLN expression in left atria tissues from C57BL/6 HOMER and µMT HOMER mice. $n = 3$ per group, two-tailed Student's *t*-test. **e**, A flow cytometric quantification of B cells, T cells and DC in the left atria from C57BL/6 mice after sham surgery, angiotensin-2 (Ang2), high-fat diet (HFD) or mitral valve regurgitation (MR). $n = 4$ per group, one-way ANOVA. **f**, Serum IgM in C57BL/6 mice after single HOMER components quantified by ELISA. $n = 5$ per group, one-way ANOVA. Data are the mean±s.e.m. with individual values for data distribution.

nature portfolio

Corresponding author(s): Steffen Pabel, Maarten Hulsmans, Matthias Nahrendorf

Last updated by author(s): Aug 14, 2025

Reporting Summary

Nature Portfolio wishes to improve the reproducibility of the work that we publish. This form provides structure for consistency and transparency in reporting. For further information on Nature Portfolio policies, see our Editorial Policies and the Editorial Policy Checklist.

Statistics

For all statistical analyses, confirm that the following items are present in the figure legend, table legend, main text, or Methods section.

n/a	Confirmed	
☐	☒	The exact sample size (*n*) for each experimental group/condition, given as a discrete number and unit of measurement
☐	☒	A statement on whether measurements were taken from distinct samples or whether the same sample was measured repeatedly
☐	☒	The statistical test(s) used AND whether they are one- or two-sided *Only common tests should be described solely by name; describe more complex techniques in the Methods section.*
☐	☒	A description of all covariates tested
☐	☒	A description of any assumptions or corrections, such as tests of normality and adjustment for multiple comparisons
☐	☒	A full description of the statistical parameters including central tendency (e.g. means) or other basic estimates (e.g. regression coefficient) AND variation (e.g. standard deviation) or associated estimates of uncertainty (e.g. confidence intervals)
☐	☒	For null hypothesis testing, the test statistic (e.g. *F*, *t*, *r*) with confidence intervals, effect sizes, degrees of freedom and *P* value noted *Give P values as exact values whenever suitable.*
☒	☐	For Bayesian analysis, information on the choice of priors and Markov chain Monte Carlo settings
☒	☐	For hierarchical and complex designs, identification of the appropriate level for tests and full reporting of outcomes
☒	☐	Estimates of effect sizes (e.g. Cohen's *d*, Pearson's *r*), indicating how they were calculated

Our web collection on statistics for biologists contains articles on many of the points above.

Software and code

Policy information about availability of computer code

Data collection	Flow cytometry data were acquired on a BD FASAria II, BD LSRII flow cytometer and Attune NxT flow cytometer (ThermoFisher Scientific). EP data were acquired with LabChart Pro v8 (AD Instruments). Optical mapping data were collected and focused onto an 80×80 charge-coupled device camera (RedShirtImaging SMQ Camera and Macroscope IIA). Blood pressures were measured with a non-invasive tail cuff system (Kent Scientific Corporation). Intracellular calcium transients were recorded using a Nikon Eclipse Ti-U inverted microscope (Nikon Instruments) and a NeuroCCDSM camera (RedShirtImaging). Confocal microscopy was executed with a Zeiss LSM800 Airyscan. Blots were scanned with an Azure Biosystems Sapphire Biomolecular imager. ELISA data were acquired with a SpectraMax iD3 (Molecular Devices) and a Tecan Spark plate reader. Real-time qPCR data was acquired with a Bio-Rad CFX96 Real-Time system. Histological slides were scanned with the NanoZoomer 2.0RS digital slide scanner (Hamamatsu).
Data analysis	Human thoracic lymph node sizes were analyzed using Slicer v5.2.2 software. Flow cytometry data were analyzed with FlowJo v10 software. EP data were analyzed using LabChart Pro v8 software (AD Instruments). Optical mapping data were analyzed with Matlab. Intracellular calcium transients were analyzed with Neuroplex (RedShirtImaging) and Clampfit v9.2 software (Molecular Devices). Confocal, histological and blotting images were analyzed with ImageJ software (National Institutes of Health). Densitometric analyses were performed with Image Lab software (Bio-Rad). Real-time qPCR data were analyzed with Bio-Rad CFX Manager v3.1. scRNAseq data were processed and analyzed using Seurat v3.1, edgeR v3.34.1 and GSEA v4.2.2.

For manuscripts utilizing custom algorithms or software that are central to the research but not yet described in published literature, software must be made available to editors and reviewers. We strongly encourage code deposition in a community repository (e.g. GitHub). See the Nature Portfolio guidelines for submitting code & software for further information.

Data

Policy information about availability of data

All manuscripts must include a data availability statement. This statement should provide the following information, where applicable:

- Accession codes, unique identifiers, or web links for publicly available datasets
- A description of any restrictions on data availability
- For clinical datasets or third party data, please ensure that the statement adheres to our policy

Raw and processed mouse scRNA-seq data as well as processed human scRNA-seq data are available at the NCBI's Gene Expression Omnibus database under accession no. GSE224959. Raw human scRNA-seq data are accessible at the controlled access repository Data Use Oversight System (DUOS; https://duos.broadinstitute.org) under accession no. DUOS-000150 under the restrictions listed by this system.

Research involving human participants, their data, or biological material

Policy information about studies with human participants or human data. See also policy information about sex, gender (identity/presentation), and sexual orientation and race, ethnicity and racism.

Reporting on sex and gender	Analysis of thoracic lymph node size was undertaken on a cohort of sex-matched patients with AF or sinus rhythm. To explore the prevalence of anti-ADRB1 in humans with and without AF, no matching for sex was attempted. No sex- and gender-based analyses were performed.
Reporting on race, ethnicity, or other socially relevant groupings	No socially constructed or socially relevant categorization variables were used in this manuscript.
Population characteristics	Key baseline characteristics are presented in Supplementary Tables 1 and 2.
Recruitment	Analysis of thoracic lymph node size was undertaken as a substudy from the Oxford Risk Factors And Non-Invasive Imaging (ORFAN) Study. A cohort of age- and sex-matched patients with AF or sinus rhythm undergoing coronary computed tomography were randomly identified from the registry arm of the ORFAN study. To explore the prevalence of anti-ADRB1 in humans with and without AF, stored frozen plasma samples were randomly selected from patients who had participated in one of two ethically approved clinical trials; all patients freely gave their written informed consent. For the sinus rhythm group, samples were selected at random from patients (n=152) who participated in the Statin Therapy in Cardiac Surgery (STICS) trial (ClinicalTrials.gov no. NCT01573143). All patients in this trial were confirmed by ECG to be in sinus rhythm at the time this sample was taken (baseline sample, prior to planned cardiac surgery and prior to trial group allocation). For the AF group, samples were selected at random from patients (n=41) participating in the LOSE-AF trial (ClinicalTrials.gov no. NCT03713775). All patients were confirmed by ECG to be in AF at the time this baseline sample was acquired. Whilst known risk factors for AF were present in patients in both trials, the inclusion/exclusion criteria differed and patients in LOSE-AF were required to have elevated body mass index to enter the study. No matching for baseline characteristics was attempted.
Ethics oversight	Analysis of thoracic lymph node size was undertaken as a substudy from the Oxford Risk Factors And Non-Invasive Imaging (ORFAN) Study (Ethics committee reference 15/SC/0545, Confidentiality Advisory Group reference 20/CAG/0157). To explore the prevalence of anti-ADRB1 in humans with and without AF, patients were randomly selected from one of two ethically approved clinical trials (STICS trial, ClinicalTrials.gov no. NCT01573143 and LOSE-AF trial, ClinicalTrials.gov no. NCT03713775); all patients freely gave their written informed consent.

Note that full information on the approval of the study protocol must also be provided in the manuscript.

Field-specific reporting

Please select the one below that is the best fit for your research. If you are not sure, read the appropriate sections before making your selection.

☒ Life sciences ☐ Behavioural & social sciences ☐ Ecological, evolutionary & environmental sciences

For a reference copy of the document with all sections, see nature.com/documents/nr-reporting-summary-flat.pdf

Life sciences study design

All studies must disclose on these points even when the disclosure is negative.

Sample size	Sample size was approximated based on prior experiments and available data (DOI:10.1126/science.abq3061) without statistical predetermination.
Data exclusions	No data were excluded.
Replication	All data were acquired during at least two independent experiments. All replication attempts were successful.
Randomization	Animals were randomly assigned to experimental groups. For in vitro experiment, cells were randomly distributed in different groups.

Blinding	All mouse experiments and downstream analyses were performed in a blinded fashion. Blinding was not possible for the in vitro experiments.

Reporting for specific materials, systems and methods

We require information from authors about some types of materials, experimental systems and methods used in many studies. Here, indicate whether each material, system or method listed is relevant to your study. If you are not sure if a list item applies to your research, read the appropriate section before selecting a response.

Materials & experimental systems

n/a	Involved in the study
☐	☒ Antibodies
☒	☐ Eukaryotic cell lines
☒	☐ Palaeontology and archaeology
☐	☒ Animals and other organisms
☒	☐ Clinical data
☒	☐ Dual use research of concern
☒	☐ Plants

Methods

n/a	Involved in the study
☒	☐ ChIP-seq
☐	☒ Flow cytometry
☒	☐ MRI-based neuroimaging

Antibodies

Antibodies used	Antibodies for flow cytometry: B220 (BioLegend, 103222, clone RA3-6B2), CD3 (BioLegend, 100206, 100209, clone 17A2. dilution 1:100), CD4 (BioLegend, 100434, clone GK1.5), CD11b (BioLegend, 101212, clone M1/70), CD11c (BioLegend, 117318, clone N418), CD19 (BioLegend, 115520, 115555, clone 6D5), CD45 (BioLegend, 103128, 103147, clone 30-F11), CD64 (BioLegend, 139306, clone X54-5/7.1), CD115 (BioLegend, 135513, clone AFS98), CD138 (BioLegend, 142510, clone 281-2), CD317 (BioLegend, 127038, clone 551/927), CXCR5 (BioLegend, 145506, clone L138D7), Fas (BioLegend, 152612, clone SA367H8), GL7 (BioLegend, 144604, clone GL7), Ly6C (BioLegend, 128036, clone HK1.4), Ly6G (BioLegend, 127606, 127641, clone 1A8), MHCII (BioLegend, 107632, clone M5/114.15.2), NK1.1 (BioLegend, 108736, clone PK136), TACI (BioLegend, 133404, clone 8F10), XCR1 (BioLegend, 148225, clone ZET), CD80 (BioLegend, 104714, clone 16-10A1), CD23 (BioLegend, 101614, clone B3B4), CD21/CD35 (BioLegend, 123420, clone 7E9), IgD (BioLegend, 405725, clone 11-26c.2a) and IgG (BioLegend, 406620, clone RMG1-1) , all dilution 1:300, unless otherwise mentioned. DAPI or LIVE/DEAD Fixable Aqua Dead Cell Stain (Life Technologies, L-34966) was used as a cell viability marker. Antibodies for immunocytochemistry, immunofluorescence, antigen immunoblotting, Western blotting and ELISA: Rabbit anti-mouse Adrb1 (Alomone Labs, AAR-023, 1:400), donkey anti-rabbit IgG Alexa Fluor 647 (ThermoFisher Scientific, A-31573, 1:1000), goat anti-mouse IgG Alexa Fluor 568 (ThermoFisher Scientific, A-11004, 1:1000), goat anti-mouse IgM Alexa Fluor 555 (ThermoFisher Scientific, A-21426, 1:100), WGA Alexa Fluor 488 (ThermoFisher Scientific, W11261, 1:100), anti-mouse Troponin I antibody (Abcam, ab47003, 1:200), goat anti-rabbit IgG Alexa Fluor 488 (ThermoFisher Scientific, A-11008, 1:100), goat anti-mouse IgM IRDye 800CW (LI-COR, 926-32280, 1:2500), anti-mouse p2808 RyR2 (Badrilla, A-010-30, 1:1000), anti-mouse RyR2 (ThermoFisher Scientific, PA5-87416, 1:15000), anti-mouse GAPDH (Cell Signaling, 2118, 1:5000), HRP-conjugated secondary antibodies (Cell Signaling, 7074, 1:5000), HRP-conjugated goat anti-mouse IgM (Abcam, ab97230, 1:10000), HRP-conjugated goat anti-mouse IgG (Abcam, ab205719, 1:10000).
Validation	All antibodies used for flow cytometry, immunocytochemistry, immunofluorescence, antigen immunoblotting, Western blotting and ELISA were previously validated for the respective application by the distributor. The use of each antibody for imaging or cytometric application can be accessed on the manufacturer's website.

Animals and other research organisms

Policy information about studies involving animals; ARRIVE guidelines recommended for reporting animal research, and Sex and Gender in Research

Laboratory animals	Wildtype C57BL/6 (stock 000664), B6.129S2-Ighmtm1Cgn/J (μMT, stock 002288), B6.C(Cg)-Cd79atm1(cre)Reth/EhobJ (Mb1-Cre, stock 020505), B6.129-Prdm1tm1Clme/J (Prdm1-fl/+, stock 008100), B6.FVB-Tg (Myh6-cre) 2182Mds/J (Myh6-Cre, stock 011038), Gt (ROSA) 26Sortm4 (ACTB-tdTomato,-EGFP)Luo/J (mTmG-fl/+, stock 007576), B6.129S2-H2dlAb1-Ea/J (MHCII-/-, stock 003584) and Adrb1tm1Bkk Adrb2tm1Bkk/J (Adrb1-/-, stock 003810) were purchased from Jackson Laboratory. All experiments were performed with 8- to 12-week-old animals and using age-matched groups. All animals were housed under 12-hour dark/light cycle under free access to food and water with a room temperature 21-23 °C.
Wild animals	No wild animals were used in the study.
Reporting on sex	All experiments were performed on male animals.
Field-collected samples	No field collected samples were used in the study.
Ethics oversight	Animal protocols were approved by the Institutional Animal Care and Use Committee at Massachusetts General Hospital (protocol

Ethics oversight	no. 2014N000078). All animal experiments were performed in compliance with relevant ethical regulations and all efforts were made to avoid suffering of animals.

Note that full information on the approval of the study protocol must also be provided in the manuscript.

Plants

Seed stocks	n/a
Novel plant genotypes	n/a
Authentication	n/a

Flow Cytometry

Plots

Confirm that:

☒ The axis labels state the marker and fluorochrome used (e.g. CD4-FITC).

☒ The axis scales are clearly visible. Include numbers along axes only for bottom left plot of group (a 'group' is an analysis of identical markers).

☒ All plots are contour plots with outliers or pseudocolor plots.

☒ A numerical value for number of cells or percentage (with statistics) is provided.

Methodology

Sample preparation	Mouse peripheral blood was collected by retro-orbital bleeding using heparinized capillary tubes, and red blood cells were lysed with 1× red blood cell lysis buffer (Biolegend). For organ harvest, an incision was made in the right atrium and mice were perfused through the left ventricle with 10 mL of ice-cold PBS. Mediastinal and iliac lymph nodes were carefully excised using a dissection microscope. Lymph nodes were then plunged and filtered through a 40-µm cell strainer. For analysis of the bone marrow, the epiphyses of the tibia were carefully opened and flushed with FACS buffer (1× PBS supplemented with 0.5% BSA). The collected bone marrow cells were then filtered through a 40-µm cell trainer. Left atrial tissues were excised using a dissection microscope, minced into small pieces and enzymatically digested with 450 U/mL collagenase I, 125 U/mL collagenase XI, 60 U/mL DNase I and 60 U/mL hyaluronidase (all Sigma-Aldrich) for 30 min at 37°C under agitation. After digestion, tissues were washed and filtered through a 40-µm cell strainer and subsequently centrifuged to obtain single-cell suspensions.
Instrument	Flow cytometry data were acquired on a BD FASAria II, BD LSRII flow cytometer and Attune NxT flow cytometer (ThermoFisher Scientific).
Software	FACS Diva v6.1 software (BD Biosciences) and Attune Cytometric v5.3.0 software (ThermoFisher Scientific) were used for data collection. Data were analyzed with FlowJo v10 software.
Cell population abundance	n/a
Gating strategy	All cell populations were pre-gated on viable and single cells. Blood B cells were gated as CD19+ B220+ CD3-, T cells as CD19- B220- CD3+, neutrophils as CD19- B220- CD3- CD11b+ CD115low/int Ly6G+ and monocytes as CD19- B220- CD3- CD11b+ CD115high Ly6G- Ly6Clow/high. Tissue pDC were gated as CD45+ CD19- CD3- Ly6G- NK1.1- CD11cint CD317+, cDC1 as CD45+ CD19- CD3- Ly6G- NK1.1- CD317- CD11c+ MHCII+ XCR1+ and cDC2 as CD45+ CD19- CD3- Ly6G- NK1.1- CD317- CD11c+ MHCII + CD11b+. Tissue B cells were gated as B220+, germinal center B cells as B220+ GL7+ Fas+, follicular helper T cells as CD3+ CD4+ PD1+ CXCR15+ and plasma cells as CD138+ TACI+, age-associated B cells as CD23- CD21- CD35-, follicular B cells as CD23+ CD21+ CD35+, plasmablasts as CD138+ B220+ CD19+, naive B cells as IgG- IgD+ and class-switched activated B cells as IgG+ IgD-.

☒ Tick this box to confirm that a figure exemplifying the gating strategy is provided in the Supplementary Information.